



Annual Report 2018

Laboratory of Environmental Chemistry

On the cover page:

Top: View of the Belukha glacier saddle, where two ice cores were drilled in 2018, from the Ak-kem basecamp (Siberian Altai, Russia).

Bottom – left to right: The 2018 Belukha ice core drilling team. View of the drill site with drill tent in front and camp (sleeping and kitchen tents) in the back when looking into Kazakhstan.

Inside the drill tent: ice core drilling in progress.

Please see report on p.31.

PAUL SCHERRER INSTITUT



Annual Report 2018

Laboratory of Environmental Chemistry

Editors

M. Schwikowski, M. Ammann

Paul Scherrer Institut

Laboratory of Environmental Chemistry

5232 Villigen PSI

Switzerland

Phone +41 56 310 25 05

www.psi.ch/luc

Reports are available: www.psi.ch/luc/annual-reports



TABLE OF CONTENTS

Editorial.....	1
Surface Chemistry	
CLOSING THE GAP IN OPEN DATA MANAGEMENT T. Bartels-Rausch.....	3
CHEMICAL MORPHOLOGY OF URBAN HAZE PARTICLES Y. Zhu, Z. Wu, J. Dou, U. K. Krieger, P. A. Alpert, P. Corral Arroyo, M. Ammann.....	4
MIXING STATE OF MARINE AEROSOL PARTICLES IMPACTED BY URBAN OUTFLOW B. Wang, J. Xue, P. Kang, X. Lin, X. Jiang, K. Gao, T. Tang, J. Dou, U. K. Krieger, P. Corral Arroyo, M. Ammann, P. A. Alpert.....	5
CHEMICAL CHANGES DURING AQUEOUS NANOPLASTICS DEGRADATION P. Passananti, P. A. Alpert, P. Corral Arroyo, B. Watts, M. Ammann, P. Rissanen, J. Dou, U. K. Krieger ..	6
IRON LEACHING FROM FERRIHYDRITE A. Boucly, L. Artiglia, H. Yang, J. P. Gabathuler, M. Ammann.....	7
FENTON CHEMISTRY AT THE LIQUID-VAPOR INTERFACE L. Artiglia, S. Chen, H. Yang, A. Boucly, J. P. Gabathuler, J. A. van Bokhoven, M. Ammann.....	8
NANOSCALE IMAGING AND MODELING OF PHOTOCHEMICAL AEROSOL AGING P. A. Alpert, P. Corral Arroyo, B. Watts, J. Raabe, M. Ammann, J. Dou, B. Luo, T. Peter, U. K. Krieger...	9
TOWARDS FE(III)-CITRATE RHEOMETRY F. Schneider, P. A. Alpert, P. Corral Arroyo, J. Edebeli, M. Ammann.....	10
LOW-VOLATILITY PRODUCTS OF IRON(III) CITRATE PHOTOCHEMISTRY P. Corral Arroyo, Y. Manoharan, K. Arturi, S. Bjelić, T. Bartels-Rausch, P. A. Alpert, M. Ammann.....	11
A CATIONIC SURFACTANT ACCELERATES BROMIDE OXIDATION S. Chen, J. Edebeli, M. Ammann.....	12
A SUBZERO TEMPERATURE ENVIRONMENTAL CELL FOR ICE NUCLEATION P. A. Alpert, S. Finizio, B. Watts, J. Raabe, C. Padeste, M. Ammann, J. Dou, U. K. Krieger.....	13
SURFACE PROPERTIES OF AN ALKYLAMMONIUM SURFACTANT S. Chen, L. Artiglia, X. Kong, H. Yang, P. Corral Arroyo, K. Roy, N. Prisle, M. Ammann.....	14
ICE NUCLEATION ACTIVITY OF FRESH AND AGED PROPANE FLAME SOOT F. Mahrt, J. Dou, U. Lohmann, Z. A. Kanji, P. A. Alpert, P. Corral Arroyo, P. Grönquist.....	15
WATER STRUCTURE IN PRESENCE OF A SURFACE ACTIVE ORGANIC SOLUTE H. Yang, L. Artiglia, J. P. Gabathuler, A. Boucly, S. Chen, M. Ammann.....	16
THE STRUCTURE OF ADSORBED WATER ON ALKALI FELDSPAR SUBSTRATES H. Yang, L. Artiglia, A. Boucly, T. Bartels-Rausch, J. P. Gabathuler, M. Ammann.....	17
LIQUID LIKE LAYER (LLL) IN THE SPOTLIGHT J. P. Gabathuler, H. Yang, L. Artiglia, A. Boucly, M. Ammann, T. Bartels-Rausch.....	18
CHEMICAL REACTIVITY DURING SNOW METAMORPHISM J. Edebeli, S. E. Avak, J. Trachsel, M. Schneebeli, A. Eichler, M. Ammann, T. Bartels-Rausch.....	19

Analytical Chemistry

BIOMASS BURNING IN THE AMAZON BASIN RECORDED IN ILLIMANI ICE CORE D. Osmont, M. Sigl, A. Eichler, T. M. Jenk, M. Schwikowski	20
6000 YEARS OF FIRE DYNAMICS FROM AN ALTAI ICE CORE D. Osmont, M. Sigl, M. Schwikowski	21
ICE RECORDS REVEAL REGIONAL FOSSIL FUEL POLLUTION S. O. Brügger, E. Gobet, M. Sigl, T. Blunier, M. Schwikowski, W. Tinner	22
MELT-INDUCED FRACTIONATION OF TRACE ELEMENTS IN ALPINE SNOW S. E. Avak, J. Trachsel, J. Edebeli, S. Brütsch, T. Bartels-Rausch, M. Schneebeli, M. Schwikowski, A. Eichler	23
A NEW METHOD FOR <i>IN SITU</i> ANALYSIS OF TRACE ELEMENTS IN GLACIER ICE S. E. Avak, M. Guillong, O. Laurent, T. Bartels-Rausch, M. Schwikowski, A. Eichler	24
TRACE ELEMENT ANALYSIS OF AN ANDEAN ICE CORE USING ICP-TOF-MS J. Stegmaier, T. M. Jenk, T. Erhardt, H. Fischer, A. Rivera, M. Schwikowski	25
SECONDARY ORGANIC AEROSOL MARKERS IN THE FIESCHERHORN ICE CORE A. Lauer, A. L. Vogel, F. Bachmeier, K. Arturi, S. Bjelić, I. El Haddad, L. Fang, M. Schwikowski	26
NOVEL ORGANIC COMPOUNDS IN THE BELUKHA ICE CORE A. King, C. Giorio, M. Kalberer, M. Schwikowski, E. Thomas, E. Wolff	27
300-YEAR ICE CORE OF DISSOLVED ORGANIC CARGON L. Fang, A. L. Vogel, T. M. Jenk, S. Szidat, M. Schwikowski	28
DATING OF THE MT. HUNTER ICE CORE FROM ALASKA L. Fang, D. Winski, K. Kretz, T. M. Jenk, M. Schwikowski	29
ACCUMULATION RATES FROM A REMOTE CENTRAL ASIAN GLACIER M. Kronenberg, A. Eichler, S. Brütsch, M. Hoelzle, H. Machguth, M. Schwikowski	30
DRILLING OF TWO NEW ICE CORES FROM BELUKHA, SIBERIAN ALTAI T. M. Jenk, M. Sigl, J. Stampfli, M. Barandun, R. Schild, T. Papina, S. Eyrikh, M. Schwikowski	31
ARCTIC ICE NUCLEATING PARTICLES OVER THE LAST CENTURIES M. Hartmann, T. Blunier, S. O. Brügger, J. Schmale, M. Schwikowski, A. L. Vogel, H. Wex, F. Stratmann	32
GIRLS ON ICE SWITZERLAND – FIELD BASED SCIENCE COURSES FOR YOUNG WOMEN M. Kronenberg, L. Hellmann, K. Naegeli, M. Schwikowski	33
List of Publications	34
Affiliation Index	36

EDITORIAL

For our Laboratory of Environmental Chemistry the year 2018 was an exciting one, with a wide range of scientific activities, among them the publication of overall 19 papers in peer-reviewed scientific journals. One of them, Sigl et al., 2018, demonstrated that industrial black carbon was not responsible for 19th century glacier retreat in the Alps as previously postulated and attracted special attention, resulting in coverage by Swiss TV (SRF Tagesschau of 20 October) and various print media.

In collaboration with the University of Zurich and the Laboratory for Catalysis and Sustainable Chemistry, the Surface Chemistry Group contributed to the extension of the Near Ambient Pressure XPS (NAPP) endstation at the SLS-NanoXAS beamline with a new analysis chamber that specifically allows investigations of the interface between a solid substrate and thin liquid. This substantially broadens the scope of the endstation for new applications.

A team of the Analytical Chemistry Group in collaboration with the Institute for Water and Environmental Problems, Barnaul, Siberia, collected two ice cores from the Belukha saddle (4062 m a.s.l., 49.81°N, 86.58°E) in the Siberian Altai. One core reached bedrock at 160 m, giving access to the oldest ice, which was not achieved during the first drilling operation at Belukha glacier in 2001. The second core was collected as heritage core to be stored in the world's first ice archive sanctuary in Antarctica in the frame of the international ICE MEMORY program.

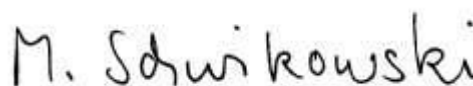
At the end of the year the 4-year SNF-Sinergia project "Paleo fires from high-alpine ice cores" finished, which was coordinated by PSI with partners from the Institute for Atmospheric and Climate Science, ETHZ, and the

Institute of Plant Sciences as well as the Institute of Geography, both University of Bern. The project produced long-term fire reconstructions from different geographical regions using black carbon and charcoal as fire tracers, provided a modelling framework to put the ice core data in a broad context, by implementing microscopic charcoal into a global climate model, and created a reference fire product for Europe from satellite data.

The year 2018 also saw a stimulating international conference on the Physics and Chemistry of Ice (PCI) with 116 participants, organized by Thorsten Bartels-Rausch and Doris Bühler, which took place at the ETHZ.

Four PhD students defended successfully, Anna Dal Farra, Pablo Corral Aroyo, and Dimitri Osmont at the University of Bern, and Jacinta Edebeli at the ETHZ. Theo Jenk, scientist in the Analytical Chemistry Group, was awarded tenure at PSI and postdoc Michael Sigl received a prestigious ERC consolidator grant for studying the timing of Holocene volcanic eruptions, which will take him to the University of Bern. Congratulations to all of them!

Our 2-days LUC retreat took us to Trogen, in the beautiful landscape of Appenzell, where we not only engaged in lively discussions about future research directions, functioning of our lab, and interactions between the two groups, but also got a lesson in traditional Appenzell dancing. For the 2018 excursion, LUC went underground on a guided tour through the Gonzen iron mine in Sargans. We concluded the year with a bowling competition in Baden.



Margit Schwikowski

CLOSING THE GAP IN OPEN DATA MANAGEMENT

T. Bartels-Rausch (PSI)

Preparing our research data for free and open accessibility has benefits for our internal project management and teamwork.

Science is based on research data being collected, analyzed and interpreted, and published (Fig. 1). To safeguard good research practice, to increase the public trust in research, and to stimulate new perspectives across scientific disciplines, the Swiss National Science Foundation expects us to manage and share research data as open as possible [1].

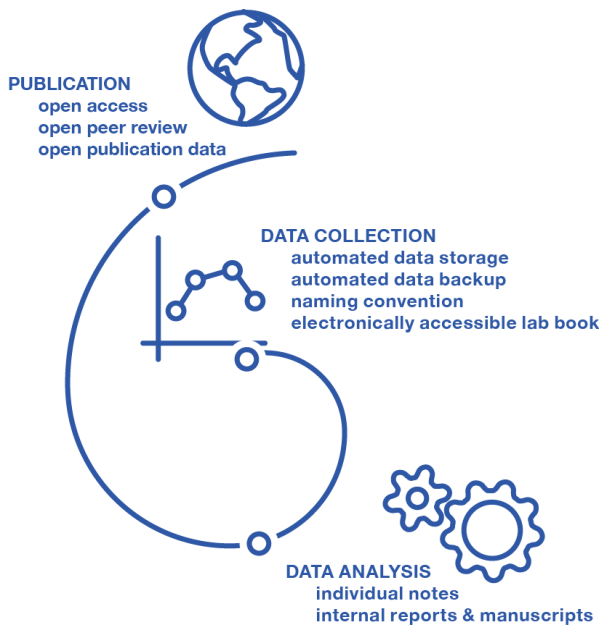


Fig. 1: Current status of data management during a project's lifetime starting with collecting the raw data and finishing with the publication of research articles.

Fig. 1 illustrates the lifecycle of research as part of a SNF funded project. This research is typically performed in small teams around a PhD student. The lifecycle reveals that currently data analysis is the weakest link in establishing open data management. Publications and their commented data are generally published open access and thus globally shared. Data collection and storage runs automated and unified naming conventions ensure efficient data handling. The data analysis and interpretation however, is still largely documented in individual notes, internal reports, and manuscripts. Curating these data for open access would require unreasonable time and effort.

One solution to establish open data analysis, is the use of repositories (Fig. 2). Repositories are data management systems that inherently record changes over time [2]. This type version control system offers several advantages [3]:

- Annotating changes is mandatory. Motivation, interpretation, and conclusions are stored along with the processed data increasing the transparency, as replication or sharing of is straightforward at any time.
- Communication with the repository server is integrated in current scientific software such as Matlab. Researchers continue working on their local computer with very little restriction on the choice of scientific software used.
- Team members can process data simultaneously and develop a common expertise in data management.

Repository systems are routinely used in complex software development, such as for Linux or by Microsoft. Thus, data processing needs to be scripted to use them for scientific projects, which undoubtedly requires some initial effort. A further benefit of scripting data analysis is – however – the ability to efficiently and rapidly analyze experiments during campaigns such as at the SLS.

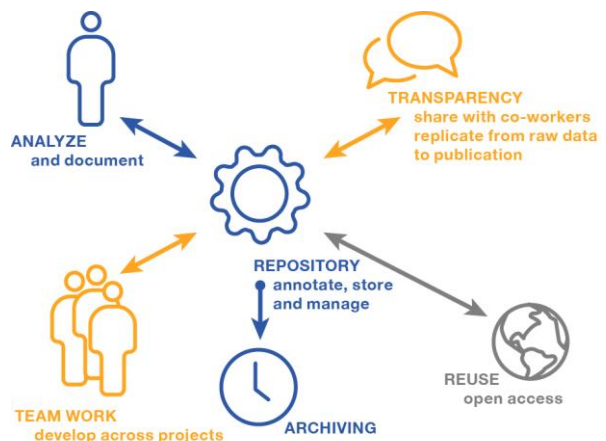


Fig. 2: Data analysis using a repository to store and manage data for standalone usage (blue), to share in teams or with co-workers (yellow), and to make curated data available open access (grey).

-
- [1] http://www.snf.ch/en/theSNSF/research-policies/open_research_data/
 [2] <https://c4science.ch>
 [3] <https://git-scm.com>

CHEMICAL MORPHOLOGY OF URBAN HAZE PARTICLES

Y. Zhu, Z. Wu (PKU), J. Dou, U. K. Krieger (ETHZ), P. A. Alpert (PSI), P. Corral Arroyo (PSI & Univ. Bern), M. Ammann (PSI)

Aerosol hygroscopicity and chemical composition on single particles from highly polluted ambient anthropogenic environments was determined to aid our understanding of their water content and cloud formation ability.

Heavy haze frequently takes place in the atmosphere of the North China Plain and threatens the health of millions of people [1]. However, the mechanisms for haze development and visibility degradation, including particle hygroscopicity, mixing state, loading of secondary aerosol formation, multiphase chemistry and the reactive uptake of gaseous molecules at the micro-level remain unclear. Atmospheric particles are chemically complex and can contain hydrophobic carbonaceous material such as soot and fresh anthropogenic emissions, but also hygroscopic salts such as sulfate and nitrate [2,3]. The morphology and chemistry of individual particles (e.g. Fig. 1) that reside in the atmosphere strongly impacts physicochemical characteristic changes of aerosol particles. We use X-ray microspectroscopy to quantify mixing of organic matter, inorganic matter, and black carbon in single particles taken from anthropogenic aerosol populations from Beijing, all with well-characterized and particle resolved hygroscopicity distributions and bulk chemical composition measured at the PKU supersite. Also, we subjected ambient samples to a high relative humidity (70%) and probed particles that do and do not take up water. Atmospheric particles collected at the PKU supersite in Beijing, China on 29 Dec. 2017 at 22:18 (GMT+8) were impacted onto silicon nitride membranes mounted in the PolLux in-situ cell, a custom built environmental microreactor.

In winter 2017, an intensive campaign was carried out at the PKU supersite. A suite of instruments including CIMS, AMS, HTDMA, SP2, CCNc, MOUDI, LIF, PTR-MS, etc. was operated simultaneously. Figure 1 (A, B, C) shows the physical and chemical properties of atmospheric particles collected at the PKU supersite. Figure 1 (D) shows sub-particle carbon speciation of a random sample of ~30 particles using X-ray microspectroscopy and note our full dataset comprises hundreds of particles. We find that all particles have organic carbon (OC), and there is significant sp²-hybridized carbon (an indicator of soot or elemental carbon, EC) and inorganic species (IN). Particles were mainly mixtures of these three components (InOCEC) at 37% of the total population. Many particles were dominated only by OC at 34%. Organic and soot dominated particles (OCEC) represented 24% of the total. The remaining 5% of the particles were InOC type.

When exposing particle to a humid air using a custom environmental cell, X-ray images revealed some particles did and did not take up water clearly identified by

a significant or no change, respectively, in oxygen absorption. Non-deliquesced (not hygroscopic) particles are suspected to contain soot or organic matter with functionalities comparably different from particles that are hygroscopic. We are now in the process of developing new image analysis techniques to automate particle identification in terms of water uptake and mixing state all while resolving particle size. Doing so will allow for a direct representation of particle resolved hygroscopic and chemical speciation to better understand light absorption, visibility, cloud formation, and pollution formation episodes in Beijing.

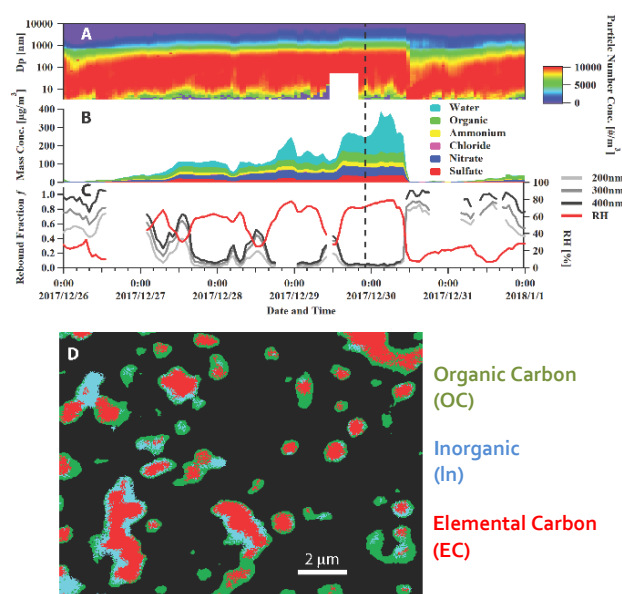


Fig. 1: (A) Size distribution normalized to particle diameter. (B) Concentration and composition of atmospheric particles collected at the PKU supersite. Water content is modelled using ISORROPIA. (C) Bounce factor of particles and ambient RH. (D) Random sample of ~30 particles showing sub-particle carbon speciation. Colors indicate dominant type OC (green), In (blue), and EC (red). Sampling time is indicated by the vertical dashed line in A-C). Scale bar is shown.

We acknowledge funding from the National Natural Science Foundation of China (Grant 41571130021 and 41875149), the European Union's Horizon 2020 research and innovation programme under the Marie Skłodowska-Curie grant agreement (701647) and the Swiss National Science Foundation (Grant 163074).

- [1] S. Guo et al., Proc. Natl. Acad. Sci. USA, **111**, 17373-17378 (2014).
- [2] D. S. Piens et al., Environ. Sci. Technol., **50**, 5172-5180 (2018).
- [3] M. Fraund et al., Atmosphere **8**, 173 (2017).

MIXING STATE OF MARINE AEROSOL PARTICLES IMPACTED BY URBAN OUTFLOW

B. Wang, J. Xue, P. Kang, X. Lin, X. Jiang, K. Gao, T. Tang (XMU), J. Dou, U. K. Krieger (ETHZ), P. Corral Arroyo (PSI & Univ. Bern), M. Ammann, P. A. Alpert (PSI)

Sea spray particles impacted by marine biota have non-soluble components with a similar chemical and morphological signature to that of aerosolized phytoplankton exudate material. This material should not play a role in water uptake, which may suppress liquid cloud formation but remain as solid substrate for ice cloud formation.

Aerosol particles are often not a single compound residing in the atmosphere, but rather a mixture of e.g. soot, organic and inorganic materials. The marine environment is a major source of atmospheric particles due to the direct emission of sea salts and biogenic/organic matter generated by bubble bursting and wave breaking [1]. A wealth of research has investigated the capability of these mixed organic/inorganic particles to act as cloud condensation and ice nuclei with implications for cloud formation and precipitation [2]. Here, we present ice nucleation and micro-spectroscopic characterization for particles generated from a mesocosm experiment in coastal water.

The mesocosm experiment was conducted in Wuyuan Bay, Xiamen, China from April to May 2018. The particles were generated by purging air into water at the base of the mesocosm to form bubbles that burst at the water surface inside. Particles were impacted into a custom-built environmental cell and exposed to 20°C in dry air or air with relative humidity, RH=80%. Particles emitted from the mesocosm had different carbon functionalities compared to marine ambient particles collected over South China Sea. The results show similar mixing state of these fresh emitted fine mode particles from the mesocosm but different in the peak absorption in R(C*=C)R bond indicating possible differences in functionality of organics in particles.

Fig. 1 shows X-ray optical density images at four energies. The first image shown in Fig. 1A was acquired at 278 eV, which is below the energy of the carbon absorption edge indicating material that is not carbon, such as aqueous sea salt solution. Fig. 1B is taken at 285.4 eV and indicates the presence of carbon unsaturation, or carbon double bonding (C=C). Notice the detailed string-like morphology, which is likely microbial exudate material or cell cytoplasm. Fig. 1C shows absorption at 288.6 eV indicating the carboxyl organic acid function (COOH). Finally, the carbon post-edge absorption at 320 eV is shown. It is important to note that the region of interest (ROI) *i* in Fig. 1A does not have any C=C absorption indicating that the unsaturated material is not detected in aqueous solution. The ROI *ii* shows a dominant C=C signature but a secondary COOH absorption is also present. We suspect the circle in ROI *iii* is a microbial cell and is dominated by COOH but has a secondary C=C signature, opposite to ROI *ii*. This indicates that cellular material in these sea

spray particles with strong C=C bonding is preferentially ejected from cells and does not absorb water.

These particles were also observed to be efficient ice nuclei. Ice nucleation experiments show particles collected from the mesocosm took up water first and formed ice via immersion mode above 227 K and nucleated ice via deposition mode (no water uptake) below 227 K. Microorganism growth was tracked over time while aerosol particles were generated. The ice nucleation ability of airborne particles was not significantly different under different biological activity. We have used electron and X-ray microspectroscopy to provide chemical speciation and mixing state of particles at an unprecedented level of microscopic detail and insight for better understanding in ice nucleation in the atmosphere over coastal and open oceans.

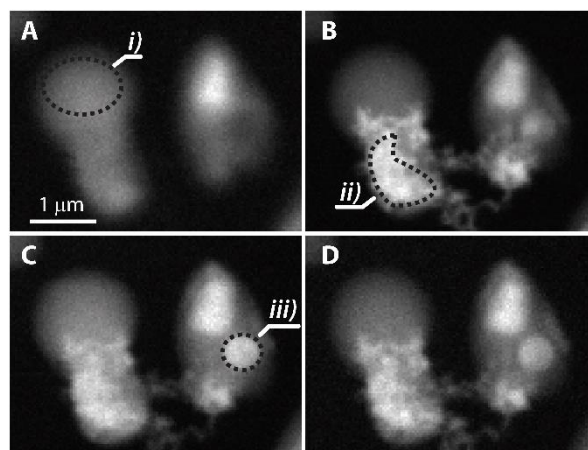


Fig. 1: X-ray optical density images acquired at (A) 278 eV, (B) 285.4 eV, (C) 288.6 eV and (D) 320 eV. Brighter pixels indicate greater absorption. Areas of interest *i*), *ii*) and *iii*) bounded by dotted black lines are discussed in the text.

We acknowledge funding from the National Natural Science Foundation of China (Grant 41775133), the Fundamental Research Funds for the Central Universities (Grant 20720160111), the European Union's Horizon 2020 research and innovation programme under the Marie Skłodowska-Curie grant agreement (701647) and the Swiss National Science Foundation (Grant 163074).

- [1] A. Laskin et al., *Annu. Rev. Anal. Chem.*, **9** (1), 117–143 (2016).
- [2] D. Knopf et al., *ACS Earth Space Chem.*, **2**, 168–202 (2018).

CHEMICAL CHANGES DURING AQUEOUS NANOPLASTICS DEGRADATION

M. Passananti (Univ. Helsinki, Univ. Tampere), P. A. Alpert (PSI), P. Corral Arroyo (PSI & Univ. Bern), B. Watts, M. Ammann (PSI), M. P. Rissanen (Univ. Helsinki), J. Dou, U. K. Krieger (ETHZ)

Nanoplastics from the Baltic Sea were chemically characterized and compared with laboratory generated polystyrene nanoparticles to understand their degradation under environmental-like conditions.

The presence of plastic material in the ocean is a major environmental problem and their occurrence and transformation in the environment is still unclear. Plastic material represents the main marine debris, and the size of this plastic debris can cover different orders of magnitude. Only recently, the presence of nanoplastics (NPs) in oceans has been demonstrated [1], and their environmental impact has remained elusive. Due to their low density, NPs are expected to float at the surface of the oceans and interact with both the atmosphere and the water body. Therefore, NPs can react with oxidants in the gas phase (e.g. ozone) and light. The objective of this project was to understand the degradation processes of NPs in the aquatic environment and to collect and analyze NPs from seawater.

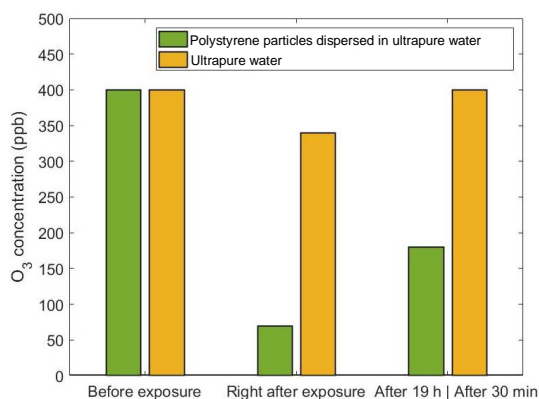


Fig. 1: Comparison between the ozone concentration at the entrance of the flow tube with that after the flow tube when either ultrapure water (yellow) and or PP dispersed in ultrapure water (green) were present in the flow tube.

We carried out experiments exposing commercially available polystyrene particles dispersed in ultrapure water to light or to ozone. The solution with polystyrene particles (PP) was placed in a flow tube and was irradiated with lamps or it was exposed to a flow of air containing 400 ppb of ozone. As shown in Fig. 1 we observed a significant uptake of ozone into the polystyrene particles, also after 19 hours of exposure. This result highlights that NPs at the surface of water can interact with oxidants in the gas phase, such as ozone. To understand the effect of ozone uptake and the interaction with light on polystyrene particles we analyzed them by Scanning transmission X-ray microscopy (STXM) coupled to near-edge X-ray absorption fine structure spectroscopy (STXM/NEXAFS).

We observed for both samples (PP exposed to light and PP exposed to ozone) the presence of oxygenated functions in the particles, showing that these plastic particles dispersed in water can react with both light and ozone.

We also collected particle samples from the Baltic Sea (Gulf of Finland) and we analyzed them by STXM/NEXAFS. We collected seawater in Helsinki's harbor, and we filtered the water on several filters with different mesh size. Finally, we extracted particles from the filters that were soluble in organic solvents, nebulized the solution and impacted the droplets onto sample substrates. The sample was analyzed by STXM/NEXAFS and as shown in Fig. 2 different regions can be identified in the analyzed particle. The red color (Fig. 2) refers to the peak at 285 eV corresponding to C=C double bonds that could be a characteristic indicator for plastic. These preliminary results show evidence for the presence of NPs in the seawater sample and promising for further studies on NPs in the environment and their reactivity.

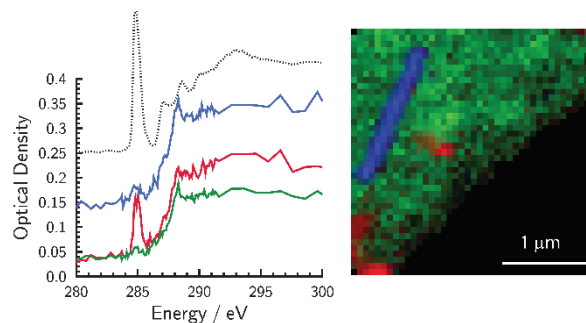


Fig. 2: X-ray spectra and image of plastic extracted from natural seawater. Spectra in the left panel are shown as blue, green and red colors, which correspond to the spatial regions in the colorized X-ray image in the right panel. For comparison, the reference spectrum of polystyrene spheres from a blank experiment is shown as the dotted line in the left panel.

We acknowledge funding from the European Research Council (Project 692891-DAMOCLES), the European Union's Horizon 2020 research and innovation programme under the Marie Skłodowska-Curie grant agreement (701647), the FoKo-CROSS project "Scanning transmission X-ray spectro-Microscopy of atmospheric particles and processes: advanced environmental cell development" co-funded by ENE and PSD research divisions at PSI, and the Swiss National Science Foundation (Grant 163074).

[1] A. Ter Halle et al., *Environ. Sci. Technol.*, **51**, 13689-13697 (2017).

IRON LEACHING FROM FERRIHYDRITE

A. Boucly (PSI), L. Artiglia (PSI LSK & LUC), H. Yang, J. P. Gabathuler (PSI & ETHZ), M. Ammann (PSI)

The leaching of iron from ferrihydrite, an iron(III) oxy-hydroxide structure, has been monitored *in situ* under different acidic conditions using X ray Photoelectron Spectroscopy (XPS) and electron yield Near Edge X-ray Absorption Fine Structure (NEXAFS) spectroscopy.

Ferrihydrite is a form of iron(III) oxy-hydroxide that exists in the form of nanoaggregates of poor crystallinity [1,2]. It has no clear structure (it exists in two types exhibiting 2 lines and 6 lines in X-ray diffractograms), has no fixed composition and is metastable [1] as it slowly transforms into either goethite or hematite. Due to its porous nanostructure, ferrihydrite has a high specific surface area [1] and offers a high number of accessible sites for adsorption and reaction. It is also considered to be the main source of bio-available iron [2] (iron that can be leached from the mineral and absorbed by organisms) and thus has a huge impact on the marine life. Ferrihydrite mainly comes from dust particles emitted from desert sand such as the Sahara. Thus, ferrihydrite can have an impact both on atmospheric chemistry as an aerosol particle and on the ocean when deposited. There is a clear lack of electron spectroscopy experiments on ferrihydrite due to its oxide and non-conductive nature; only few experiments were carried out to study its reactivity as an aerosol particle. Yet it is part of the important Fe(II)-Fe(III) redox couple, which interacts with different other redox active systems, such as reactive oxygen species (ROS) and secondary organic compounds associated with mineral dust aerosol particles. For those reasons, a first XPS and NEXAFS experiment to study the iron leaching and modification of the ferrihydrite surface is reported here.

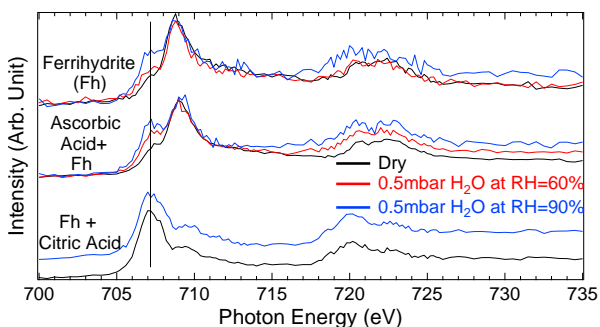


Fig. 1: Fe $L_{2,3}$ Edge NEXAFS spectra of ferrihydrite (top), ferrihydrite with ascorbic acid (middle) and ferrihydrite with citric acid (bottom). Black, red and blue lines correspond to dry state, RH=60% and RH=90%, respectively.

Three different samples have been analyzed with the *in situ* electron spectroscopy endstation at the NanoXAS beamline (SLS). The first sample is ferrihydrite alone, the second ferrihydrite with a small quantity of ascorbic

acid (a tenth of the ferrihydrite by weight) that acts to reduce the iron leached. The third sample is an aged solution of ferrihydrite dispersed in an excess amount of citric acid. Here the acid is not expected to reduce the iron leached but rather forms a stable complex with it. The spectra were acquired under three different conditions: Dry condition, 60% relative humidity (RH) at 0.5 mbar (-22.25°C) and 90% RH at 0.5 mbar (-26.25°C).

Fig. 1 shows the NEXAFS spectra of this first experiment. XPS results (not shown) provide consistent information. Under dry conditions, the slurry of ferrihydrite with citric acid shows a different chemical composition. Indeed, it features an iron(II) state while both ferrihydrite alone and ferrihydrite with ascorbic acid are dominated by iron(III) species. Yet with increasing humidity, the peak corresponding to the iron(II) state (indicated by a bar at 707 eV) increases for both ferrihydrite and ferrihydrite with ascorbic acid. While this is expected for ferrihydrite with ascorbic acid due to its reducing nature, it is much more surprising for ferrihydrite with just water as it should have stayed in an iron(III) state, or for ferrihydrite mixed with citric acid. This change in oxidation state is likely due to a beam induced effect, since iron complexes are known to undergo ligand to metal charge transfer upon absorption of photons already in the near UV range. Indeed, measurements done with liquid-jet XPS (no beam effects due to fast renewal of the solution, not shown) with solutions separated from the ferrihydrite after leaching show that the iron after leaching is in the iron(III) state for citric acid solution but in the iron(II) state for ascorbic acid. Yet this beam effect is not visible under dry conditions when all iron atoms are still within the ferrihydrite structure. This first experiment shows that a small amount of water can already modify the surface of the ferrihydrite by leaching iron, iron that can then react with species in its environment. This is interesting from the aerosol particle point of view as this available iron can be converted back to an iron (II) through photochemical processes forming the redox couple and thus be able to do redox reactions with other airborne species such as H_2O_2 or secondary organic compounds.

We acknowledge funding from the Interlaboratory Postdoc program of the ENE division.

- [1] U. Schwertmann et al., *J Colloid Interface Sci.*, **209**, 215-223 (1999).
- [2] C. Rodriguez-Navarro et al., *Atmos. Chem. Phys.*, **18**, 10089-10122 (2018).

FENTON CHEMISTRY AT THE LIQUID-VAPOR INTERFACE

L. Artiglia (PSI LSK & LUC), S. Chen, H. Yang (PSI & ETHZ), J. P. Gabathuler (PSI & ETHZ), A. Boucly (PSI), J. A. van Bokhoven (PSI LSK & ETHZ), M. Ammann (PSI)

This work shows a new approach to characterize Fenton's reagents at the liquid-vapor interface by means of liquid-jet X-ray photoelectron spectroscopy.

The Fenton's reaction produces either highly-valent iron species (ferryl, FeO^{2+}) or Fe^{3+} and $\cdot\text{OH}$ radicals. The study of Fenton chemistry is of wide interest, due to the presence of Fe^{2+} and peroxides both in vivo and in the environment (atmosphere, water, and soils). The mechanism at the basis of Fenton reactions has not been fully understood yet. Depending on the reaction conditions, the Fe^{2+} ions undergo either a one-electron transfer (producing Fe^{3+} and $\cdot\text{OH}$ radicals) [1] or a two-electron oxidation (yielding high-valent FeO^{2+} species) [2]. The preferential formation of either ferryls or Fe^{3+} reflects on the course of oxidative chemistry. As an example, recent experiments claim that, due to the partial hydration sphere of Fe^{2+} at the water-air interface, ferryls are preferentially formed while hydrogen peroxide is dosed from the gas phase [3]. The aim of this work is to use surface sensitive techniques (X-ray photoelectron spectroscopy XPS and electron yield near edge X-ray absorption fine structure spectroscopy NEXAFS) to investigate Fenton's reagents solutions. Photoemission spectra were acquired on liquid filaments (diameter of approx. 25 μm) generated in vacuum (base pressure 10^{-4} - 10^{-3} mbar) by means of a commercial quartz nozzle injector. Because the liquid surface exposed to the high flux x-rays (SIM beamline, Swiss Light Source) is continuously renewed, the beam damage is negligible.

We acquired the photoemission and absorption spectra of various samples starting from two concentrations of Fe^{2+} , 300 and 500 mM, respectively: reference solutions (Fe^{2+} and Fe^{3+}) and Fenton's reagents (mixtures of Fe^{2+} and hydrogen peroxide) having different $[\text{Fe}^{2+}]/[\text{H}_2\text{O}_2]$ ratios (ranging from 3:1 to 1:4). The photoemission spectra of the Fe 2p levels are shown in Fig. 1. As expected, the spectra of the two reference solutions show a positive chemical shift (about 3.2 eV) between the peak centroids. This is due to the change of the oxidation state of Fe from 2+ to 3+. The same binding energy shift is detected passing from 3:1 to 1:4 $[\text{Fe}^{2+}]/[\text{H}_2\text{O}_2]$ ratio of the Fenton's reagents. In particular, the spectrum acquired in excess of Fe^{2+} (3:1 ratio) shows a light peak broadening toward higher binding energy both at 300 and 500 mM, while the main component is still Fe^{2+} . In the case of 300 mM Fe^{2+} , only after addition of a large excess of H_2O_2 (1:4 ratio), the Fe 2p spectrum matches that of Fe^{3+} . The spectrum corresponding to the 1:1 ratio is broader, probably due to the presence of Fe^{3+} and other reaction products (e.g. iron hydroxides). In the case of 500 mM Fe^{2+} , the photoemission spectrum of the 1:1 Fenton reagent is showing an almost quantitative oxidation of Fe^{2+} to Fe^{3+} . This might suggest that the reactivity also depends on the initial concentration

of Fe^{2+} . The NEXAFS spectra are in good agreement with the results of photoemission, apart for those of the 3:1 Fenton's reagent. Relevant changes as compared to the spectrum of the reference Fe^{2+} solution are present, suggesting a significant oxidation of Fe^{2+} to Fe^{3+} , whereas XPS shows that only a small fraction of Fe^{2+} oxidizes to Fe^{3+} . Such a difference could be explained by the different probed depth of XPS and NEXAFS, the latter being more bulk sensitive due to larger kinetic energy of inelastically scattered Auger electrons (585 eV) than that of XPS (280 eV). Within the information depth of XPS, iron has a ferrous-like behavior, whereas in the bulk it is more ferric-like (NEXAFS).

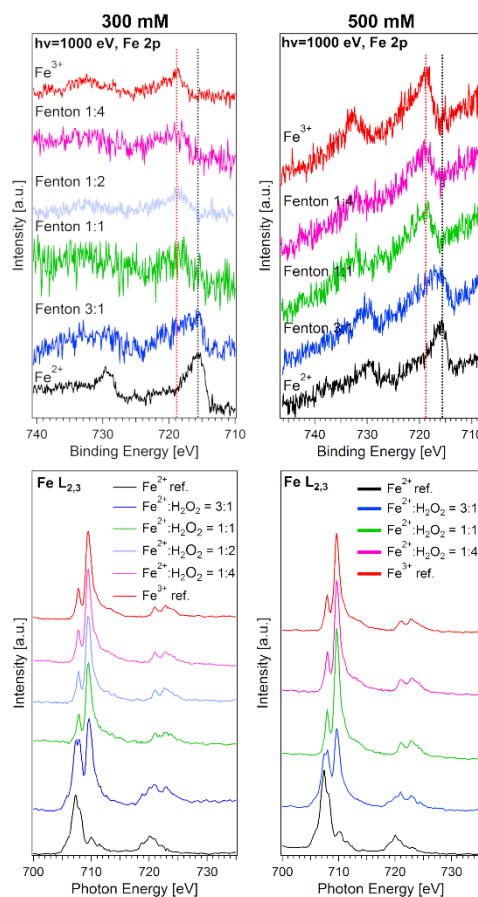


Fig. 1: (left) Fe 2p photoemission spectra and X-ray absorption spectra of the reference solutions (Fe^{2+} and Fe^{3+}) and of Fenton's reagents, 300 mM concentration; (right) Fe 2p photoemission spectra and X-ray absorption spectra of the reference solutions (Fe^{2+} and Fe^{3+}) and of Fenton's reagents, 500 mM concentration.

- [1] F. Haber, J. Weiss, Proc. Roy. Soc. A, **134**, 332-351 (1934).
- [2] W. C. Bray, M. H. Gorin, J. Amer. Chem. Soc., **54**, 2124-2125 (1932).
- [3] S. Enami et al., PNAS **111**, 623-628 (2011).

NANOSCALE IMAGING AND MODELING OF PHOTOCHEMICAL AEROSOL AGING

P. A. Alpert (PSI), P. Corral Arroyo (PSI & Univ. Bern), B. Watts, J. Raabe, M. Ammann (PSI), J. Dou, B. Luo, T. Peter, U. K. Krieger (ETHZ)

Photochemical reactions in viscous organic aerosol particles can generate radicals with low diffusivity meaning that free radicals (FRs) and reactive oxygen species (ROS) can exist for a long time in particles we breathe. They both lead to oxidative stress in human lungs when inhaled.

Major radical sources in atmospheric aerosol particles are photolysis and reactions involving trace metals [1]. Organics are ubiquitous in particles, and high iron concentration has been observed in 5% of particles [2]. Organic acids are a type of oxygenated organic matter in secondary organic aerosol, and can be removed due to photolysis reactions when they complex with Fe [3]. We use Fe-citrate (FeCit), a complex of Fe(III) and citric acid (CA), as a model system and initiate photochemical reactions using UV light at 370 nm. In a humid atmosphere containing O₂, UV light should reduce Fe(III) to Fe(II) and form a carbon centered FR. This should then react with O₂ to form HO₂, H₂O₂ and OH, all of which are ROS that reoxidize iron back to Fe(III). Micro- and submicrometer sized particles of FeCit:CA at 1:1 mole ratio are placed into a custom-built environmental cell mounted in the PolLux endstation at the Swiss Light Source, irradiated for 15 min, and investigated with X-ray spectro-microscopy to observe the spatially resolved Fe oxidation state after UV was switched off.

Fig. 1 shows 2-D profiles of Fe(III) fraction as a function of relative humidity, *RH*, and time, *t*, after UV was switched off. At *RH*=40% (Fig. 1a), Fe is reduced, however reoxidation over *t* does not occur despite oxygen being present. For *RH*=50 and 60% (Fig. 1b and c), more dark reoxidation was observed.

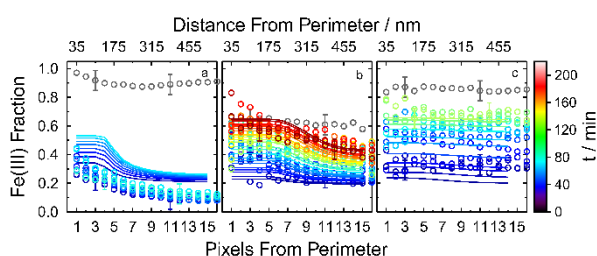


Fig. 1: 2-D profiles of the Fe(III) fraction of particles as a function of time after UV light was switched off in the color scale and for (a) *RH*=40%, (b) *RH*=50% and (c) *RH*=60%. Symbols are observations from X-ray micro-spectroscopy. Model results are shown as lines. Grey symbols indicate the Fe(III) fraction prior to UV illumination for 15 min.

This implies that organic carbon-centered radicals are being produced at low *RH*, but not reacting with oxygen to produce ROS. More reoxidation of Fe(II) requires more oxygen reaction and greater ROS production. It is

important to note that greater molecular diffusion is expected at high *RH* evident from flattening of the Fe(III) fraction profiles in Fig. 1c. Model derived profiles are shown as the solid lines and reproduce the general trend of our data.

In turn, we can calculate the production of FR and ROS in a simulated aerosol population where 5% of particles contained FeCit:CA at 1:20 mole ratio, which is similar to previous studies [2]. We report carbon centered FR and ROS concentration after 90 min of sunlight illumination in Fig. 2. We have found that FRs and ROS reach about 10¹² and 10¹¹ (molecules) μg⁻¹, respectively, of aerosol mass. In comparison, previous measurements of ambient environmentally persistent FRs and ROS were found in aerosol particles on the order of 10¹¹ μg⁻¹ [4]. This work has vast implications for damaging health effects due to particles thought not to be hazardous. Sea spray contains organics and variety of trace metals and salts, and photochemical reactions are speculated here to generate radicals which can cause damage to lungs.

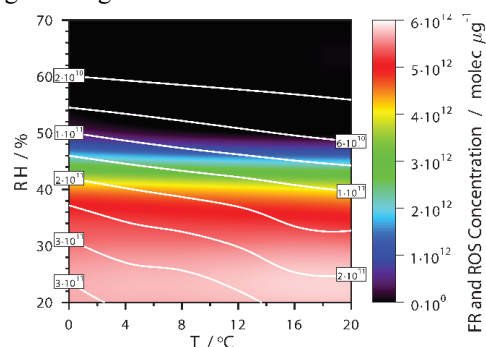


Fig. 2: Concentration of radicals in aerosol particles as a function of *T* and *RH* after 90 min of constant sunlight illumination at the Earth's surface. Free radicals (FR) and reactive oxygen species (ROS) are given as the color scale and contours, respectively.

We acknowledge funding from the FoKo-CROSS project co-funded by ENE and PSD research divisions at PSI, the European Union's Horizon 2020 research and innovation programme under the Marie Skłodowska-Curie grant agreement (701647) and the Swiss National Science Foundation (Grant 163074).

- [1] A. Tilgner et al., *J. Atmos. Chem.*, **70**, 221-256 (2013).
- [2] R. C. Moffet et al., *J. Geophys. Res.*, **117**, D07204 (2018).
- [3] C. Weller et al., *Environ. Sci. Technol.*, **48**, 5652-5659 (2014).
- [4] A. M. Arangio et al., *Atmos. Chem. Phys.*, **16**, 13105-13119 (2016).

TOWARDS FE(III)-CITRATE RHEOMETRY

F. Schneider (PSI & Univ. Bern), P. A. Alpert (PSI), P. Corral Arroyo (PSI & Univ. Bern), J. Edebeli (PSI & ETHZ), M. Ammann (PSI)

We present results from viscosity measurements of ferrous citrate in citric acid to understand the link between chemical aging and the microphysical properties of aerosol particles.

Aerosol aging is a term for chemical and physical transformations of airborne particles. It plays a major role in how aerosol particles affect climate, air quality and health. If atmospheric particles contain chromophores, indirect photochemical processes become possible, meaning that the chromophore excited by light will form a radical only through reaction with neighboring molecules (light absorption does not directly generate radicals). This is a mechanism by which redox processes of non-light absorbing molecules are catalyzed. Indirect photochemistry is particularly important in environments with insufficient UV light intensity, such as the lower troposphere at high latitudes or in twilight, where direct photolysis and radical production is inefficient. Fe(III) carboxylate is an atmospheric surrogate metal-organic complex and an example compound that can absorb light up to 500 nm. After absorption, reaction leads to the reduction of Fe(III) to Fe(II), the oxidation of the carboxylate ligand. In a collaborative project between PSI and ETH, we investigate the ability of photochemical reactions to proceed as a function of relative humidity, RH , on which particle viscosity, η , and thus, molecular diffusion is highly dependent.

Using a rheometer, η of citric acid (CA) and Fe(III)-citrate in CA, referred to as FeCit, with mole ratios of 1:1 and 1:20 were observed. Two measurement approaches were used, 1) weight-fraction, w , based, in which a solution with known w was prepared and immediately tested and 2) RH based in which a solution was left to equilibrate with RH over a long time. For CA samples, w was converted to RH using previous derivations [1,2]. For FeCit, we derived our parameterization of RH versus w . This was done following a unique experimental procedure. First, a solution with known w was prepared. Second, the solution was placed in the rheometer at some defined RH and its η was measured immediately. The RH was never optimal initially (but always close within $\pm 5\%$) and would condense (RH too high) or evaporate (RH too low) water over time leading to a more dilute or concentrated solution, respectively. This led to an unknown change of w over time, but a measureable decrease and increase in η . Finally, the RH was manually adjusted so that η over a long time (~ 4 hr) was maintained constant and matched the initial value. This long time was necessary to allow the sample to equilibrate with RH , i.e. no net increase or decrease in water content. Therefore, after the adjustment was completed, initial and final values of η were identical, and the final RH exactly corresponded to the initial w of the solution.

Fig. 1 shows η as a function of RH . Our data for CA are in perfect agreement with previous results revealing the correctness of our procedure. Values of η for FeCit tended to increase when weight fraction increased, similar to CA samples. We also found that η of FeCit at 1:20 ratio was similar to CA. At 1:1 FeCit mole ratio, η was significantly higher than 1:20. The metal-organic complex has a higher viscosity than the organic acid alone. We suspect that Van der Waals intermolecular forces such as hydrogen bonding or dipole interactions may be responsible for the greater observed η .

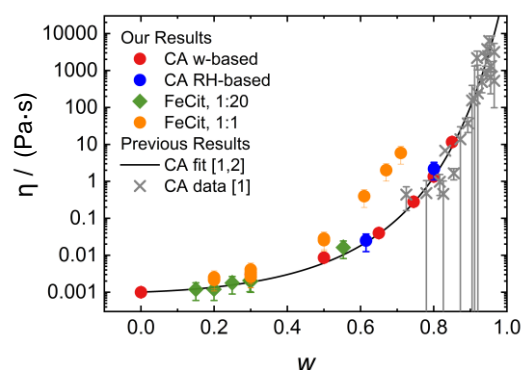


Fig. 1: Viscosity, η , of citric acid (CA) and mixed Fe-citrate and CA solutions (FeCit) as a function of weight fraction with water, w . Mole fractions of 1:1 and 1:20 (Fe(III)-citrate:CA) are indicated. Measurement methods w -based and RH -based are described in the text.

Our results have implications for chemical aging and atmospheric chemical and photochemical reactions. Typically, photochemical aging produces radicals, and an increase in η tends toward a decrease in molecular diffusion. If the molecular diffusion of radicals is reduced, their ability to move through particles decreases and they can become effectively trapped. This leads to long radical lifetime and a slowdown of reaction cycling. Also, when particles with trapped radicals are inhaled, it could be damaging to human health.

We acknowledge funding from the Swiss National Science Foundation (Grant 163074) and the European Union's Horizon 2020 research and innovation programme under the Marie Skłodowska-Curie grant agreement (701647).

- [1] D. M. Lienhard et al., *J. Phys. Chem. A*, **116**, 9954–9968 (2012).
 [2] F. H. Marshall et al., *Chem. Sci.*, **7**, 1298 (2016).

LOW-VOLATILITY PRODUCTS OF IRON(III) CITRATE PHOTOCHEMISTRY

P. Corral Arroyo, Y. Manoharan (PSI & Univ. Bern), K. Arturi, S. Bjelić (PSI LBK), T. Bartels-Rausch, P. A. Alpert, M. Ammann (PSI)

Iron (Fe) photochemistry is a major sink for carboxylic acids in aerosol particles [1]. This work investigates the products of the degradation of citric acid (CA) initiated by photolysis of Fe(III) citrate complexes by HPLC-MS.

Fe(III) carboxylate (citrate among them) complexes absorb light below about 500 nm, which is followed by ligand to metal charge transfer resulting in the reduction of iron to Fe(II) and oxidation of the carboxylate ligands, which represents a major contribution to the degradation of carboxylic acids in the atmosphere and to aerosol aging via secondary radical cycles [1].

We deposited mixtures of Fe(III) citrate (FeCit) and CA (1:1) on the surface of a petri dish, which was then exposed to UV light (centered at 350 nm) for varying times (from minutes to hours) at 40% relative humidity (RH) in synthetic air at ambient temperature and pressure. After irradiation, we extracted the film with a mixture of water and acetonitrile (1:1). Vanillin was added to the extract as internal standard. The analysis was performed with a UHPLC-HRMS using an ESI source.

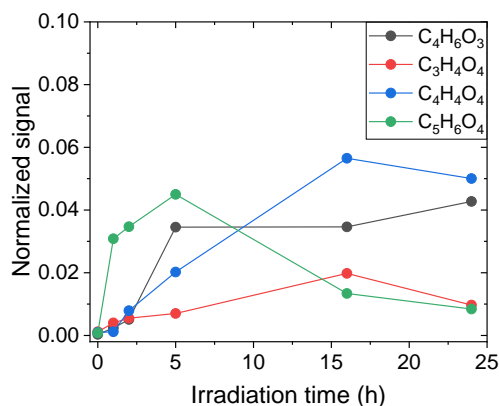


Fig. 1: Selected C3 to C5 oxidation products from the degradation of citric acid initiated by iron citrate photolysis.

We observed that the citric acid concentration decreased (not shown) during irradiation, first sharply, then much more slowly. Fig. 1 shows selected products representative of different oxidation generations exhibiting different behavior as a function of time. The C₆ compounds come from the functionalization of CA, and C₅, C₄ and C₃ compounds come from the fragmentation and further reaction following decarboxylation of the citrate ligand after initial photolysis of iron citrate complexes or by the degradation of uncomplexed CA by HOx radicals generated in the complex degradation. The general trend is an increase over the first 16 hours of irradiation and a decrease after that, most likely due to further degradation towards oxygenated volatile organic compounds (OVOCs) that leave the sample.

Release of species such as acetaldehyde or acetic acid has also been observed in separate experiments (not shown) [2].

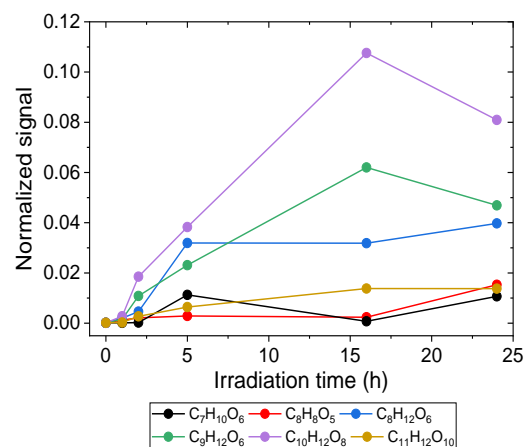


Fig. 2: Selected C7 to C11 products from secondary chemistry following the degradation of citric acid initiated by iron citrate photolysis.

Fig. 2 shows several products resulting from accretion reactions, likely produced by radical-radical recombination, or oligomerization reactions. We also found evidence for compounds with higher masses, indicating the presence of poly-iron complexes, which may have an impact on the viscosity and thus diffusivity in the system. Some of the products, e.g., C₄H₆O₂ (not shown) contain a double bond, and are indicative of oxygen deficient conditions induced by diffusion limitation of molecular oxygen otherwise needed to drive peroxy radical chemistry. At 40% RH, the viscosity of citric acid is high enough, so that the diffusivity of O₂ may get rather low. The poor supply with O₂ may become key for the secondary chemistry of this system.

We acknowledge funding from the Swiss National Science Foundation (Grant 163074) and the interlaboratory postdoc program of the ENE division, project "Analysis of organic compounds from energy production to environment".

- [1] C. Weller et al., *Environ. Sci. Technol.*, **48**, 5652-5659 (2014).
- [2] M. J. Liu et al., *J. Phys. Chem. A*, **121**, 5856-5870 (2017).

A CATIONIC SURFACTANT ACCELERATES BROMIDE OXIDATION

S. Chen, J. Edebeli (PSI & ETHZ), M. Ammann (PSI)

The reaction of ozone with sea-salt derived bromide is relevant for marine boundary layer chemistry. This study shows an obvious enhancement of ozone uptake to bromide solutions in presence of a cationic alkylammonium surfactant.

The multiphase reaction of bromide with ozone is an important bromide oxidation pathway, which later drives ozone depleting chemistry in the gas phase of marine air masses. The reaction exhibits an enhanced rate at the surface [1]. The ocean surface water and sea spray aerosol contain organic compounds, which may have a significant effect on the distribution of halide ions at the interface [2]. We selected tetrabutylammonium (TBA) for this study as a proxy for cationic surfactants deriving from biogenic oceanic material.

Solutions composed of 0.1 M TBA bromide (TBA-Br) / 0.55 M NaCl, 0.1 M TBA-Br only, 0.1 M NaBr / 0.55 M NaCl, and 0.1 M NaBr only, were used, respectively. TBA is expected to exhibit a surface excess of around 2.3×10^{14} molecule per cm^2 at 0.1 M [3]. The uptake coefficient of O_3 (γ_{obs}) is derived from the observed fractional loss of O_3 over a trough containing the aforementioned solutions and housed in a temperature-controlled reactor. In equ. 1, ω_{O_3} is the mean thermal velocity of the O_3 molecules in the gas phase (cm s^{-1}), $[\text{O}_3, \text{bypass}]$ is the measured O_3 concentration delivered to the reactor. $[\text{O}_3, \text{reactor}]$ is the O_3 concentration downstream of the reactor. Q is the flow rate of the gas passing through the reactor ($\text{cm}^3 \text{s}^{-1}$). SA is the total surface area of the solution (cm^2).

$$\gamma_{\text{obs}} = \frac{4 \cdot Q}{\omega_{\text{O}_3} \cdot SA_{\text{reactor}}} \times \ln\left(\frac{[\text{O}_3, \text{bypass}]}{[\text{O}_3, \text{reactor}]}\right) \quad (1)$$

Fig. 1 shows the measured O_3 uptake coefficients at 277 K as a function of O_3 concentration in the gas phase. Lines are fits with a kinetic model consisting of a combination of a surface reaction and a reaction-diffusion mechanism in the bulk [1]. At high O_3 concentration (above 200 ppb), γ_{obs} is constant, whereas at low atmospherically relevant O_3 concentration (between 30 and 100 ppb), γ_{obs} is decreasing. In previous studies [1,4], this behaviour has been attributed to a surface reaction dominating at low O_3 concentration. It results from the fact that the maximum coverage of O_3 on the surface is limited, which leads to the surface reaction rate saturating with higher O_3 concentration. This is not the case for the bulk phase reaction, since the bulk phase concentration of O_3 scales linearly with the gas phase concentration (Henry's law) in the relevant concentration range. The behaviour of the uptake coefficient shown in Fig. 1 is the result of the combination of parallel reaction in the bulk and reaction on the surface. The measured γ_{obs} in absence of TBA are consistent with previous studies from our group [1] and the work

by Oldridge and Abbatt [4]. The difference between the pure NaBr and the mixed NaBr/NaCl solutions may be explained by the lower solubility of O_3 due to salting out by NaCl. In presence of TBA, the O_3 uptake coefficient is higher than on the pure NaBr and NaBr/NaCl mixed solutions at low O_3 concentration, whereas they tend to be similar at high O_3 concentration. In presence of TBA, the effect of NaCl is not apparent at low O_3 concentration, which may be due to the fact that the concentration of the $[\text{Br} \cdot \text{OOO}]^-$ intermediate at the interface is independent of the presence of NaCl. However, at high O_3 concentration, a lower O_3 uptake coefficient was observed due to the salting out effect for the bulk reaction.

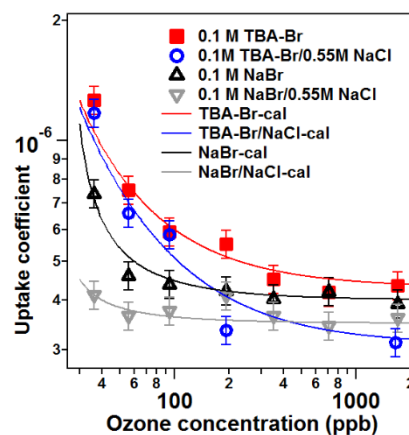


Fig. 1: Uptake coefficients of ozone as a function of ozone concentration in the gas phase.

It appears that the positively charged ammonium group in TBA helps to attract Br^- ions to the interface and possibly also leads to enhanced and saturated surface concentration of the $[\text{Br} \cdot \text{OOO}]^-$ intermediate that limits the reaction rate [1]. The salting out effect by NaCl is observed in the solution in presence of TBA. Further, such enhanced O_3 uptake on the surface is also in agreement with the liquid-jet XPS results.

We acknowledge funding from the Swiss National Science Foundation (Grant 169176).

- [1] L. Artiglia et al., *Nature. Comm.*, **8**, 700 (2017).
- [2] M.-T. Lee et al., *J. Phys. Chem. A*, **119**, 4600-4608 (2015).
- [3] J. Mata et al., *Coll. Surf. A*, **245**, 69-73 (2004).
- [4] N. Oldridge et al., *J. Phys. Chem. A*, **115**, 2590-2598 (2011).

A SUBZERO TEMPERATURE ENVIRONMENTAL CELL FOR ICE NUCLEATION

P. A. Alpert (PSI), S. Finizio, B. Watts, J. Raabe (PSI LSC), C. Padeste (PSI LMN), M. Ammann (PSI), J. Dou, U. K. Krieger (ETHZ)

A prototype of a new subzero temperature environmental cell, known as the ICE cell, was developed to probe the temperature and RH at which ice forms on single aerosol particles with nanometer scale detection to investigate the chemical and morphological characteristics of ice nucleating surfaces.

Clouds with ice particles cover about 30% of the Earth's surface at any given time. The ice particles impact cloud lifetime, precipitation, global cloud radiative forcing and thus climate. Although the ice nucleation is heavily studied, atmospheric understanding and prediction is currently insufficient due to the chemical and morphological complexity of aerosol particles from which ice nucleation is initiated [1]. Ice is known to form from 1) cloud or aqueous solution droplets, 2) on insoluble particles in droplets, 3) on particles sticking out of droplets, 4) due to surfactant molecular layers at the air water interface of droplets, 5) on dry particles (i.e. no droplets) directly from the vapor phase, or 6) through a two-step process of liquid water condensation and then freezing. Atmospheric particles can be crystalline minerals and salts, biogenic, metallic, soot, and all coated by organic matter and aged over time with atmospheric reactants [2]. We are using state of the art lithography and microfluidic technology to construct apparatus capable of capturing ice nucleation on spatial scales relevant to atmospheric particles, which are nanometers to micrometers. Doing so will allow us to observe various ice nucleating scenarios, e.g. if organic matter coatings nucleate ice or the particle core itself is responsible (see Fig. 1).

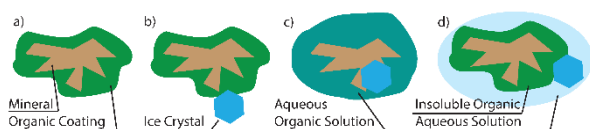


Fig. 1: Scheme of some ice nucleation pathways from (a) an organic coated mineral particle. Ice can form (b) on the surface of the organic. If the organic is liquid or soluble, water can move through it and (c) form on the mineral. If water condensation occurs but some organic is insoluble, ice may again (d) form on the organic surface.

Our prototype ICE cell was fabricated with a patterned Pt temperature sensor on a silicon nitride (SiN) membrane and a gas dosing system of humidified helium. Figure 2 shows a coarse X-ray image of the Pt sensor. Cooling of the cell was accomplished using a cold air jet directed on the membrane. The ICE cell was taken to the PolLux beamline at the Swiss Light Source for scanning transmission X-ray microscopy (STXM) measurements. It is vital for any ice nucleation apparatus that the coldest point along the path of the humidified air is where ice nucleation is desired to occur. For

the STXM, this coldest spot should be on the SiN membrane. This is difficult because the membrane thickness of 50 nm required for X-ray transmission leads to very poor thermal conductivity that limits heat transfer away from the observed ice nucleation area.

We performed an experiment in which water condensation occurred on a membrane at a relative humidity of 100% and observed the spatial extent of where droplets formed to evaluate a qualitative measure of the temperature gradient across the surface. Fig. 2 shows a collection of water droplets across the membrane surface however, this does not extend to the silicon support (not X-ray transparent) seen as a black boarder on the image edges.

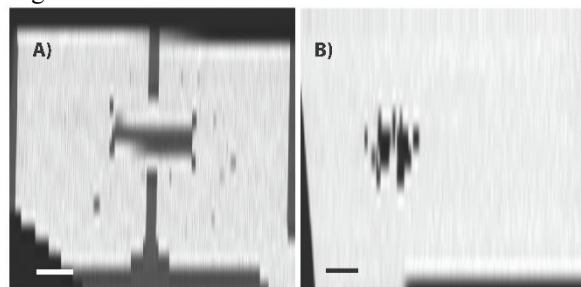


Fig. 2: STXM image of water condensation on SiN membranes. Droplets are scattered dark pixels. (A) 1x1 mm membrane with a Pt wire and contacts seen as large rectangular structures. Scale bar is 100 μm . (B) 0.5x0.5 mm membrane. Scale bar is 50 μm .

Droplets in Fig. 2A are distributed nearly uniformly about 0.8 mm across the membrane surface implying a homogenous temperature gradient. This is largely due to the use of a 40 nm Al layer evaporated on the reverse side of the membrane to achieve good thermal conductivity. In contrast, the collection of droplets seen in Fig. 2B was only about 0.1 mm across, implying a highly localized and sharp temperature gradient. This was because this membrane lacked an Al layer. Future development and use of laboratory generated and ambient particles will be realized for ice nucleation experiments.

We acknowledge funding from the FoKo-CROSS project "Scanning transmission X-ray spectro-Microscopy of atmospheric particles and processes: advanced environmental cell development" co-funded by ENE and PSD research divisions at PSI and the European Union's Horizon 2020 research and innovation programme under the Marie Skłodowska-Curie grant agreement (701647).

- [1] D. A. Knopf, P. A. Alpert, B. Wang, *ACS Earth Space Sci.*, **2**, 168-202 (2018).
- [2] A. Laskin et al., *Annu. Rev. Anal. Chem.*, **9**, 117-143 (2016).

SURFACE PROPERTIES OF AN ALKYLAMMONIUM SURFACTANT

S. Chen (PSI & ETHZ), L. Artiglia (PSI LSK & LUC), X. Kong (Univ. Oulu), H. Yang (PSI & ETHZ), P. Corral Arroyo (PSI & Univ. Bern), K. Roy (ETHZ), N. Prisle (Univ. Oulu), M. Ammann (PSI)

The oxidation of bromide by ozone in seawater, sea spray or marine aerosol occurs preferentially at the interface. Here, we assess the surface propensity of bromide in presence of the cationic surfactant tetrabutylammonium at the liquid-vapor interface by liquid-jet XPS.

Oxidation of bromide to hypobromite is one of the important reactions to produce molecular halogen compounds that later drive O₃ depleting chemistry in the troposphere [1]. The reaction shows a strong preference for the liquid-vapor interface [2] and is thus sensitive to the interfacial density of bromide. The latter may be affected by surface active organics ubiquitously present at the ocean surface together with the inorganic ‘sea salts’. Here, we use liquid-jet X-ray photoelectron spectroscopy (XPS) at SLS [3] to assess the surface propensity of bromide in presence of tetrabutylammonium (TBA) bromide.

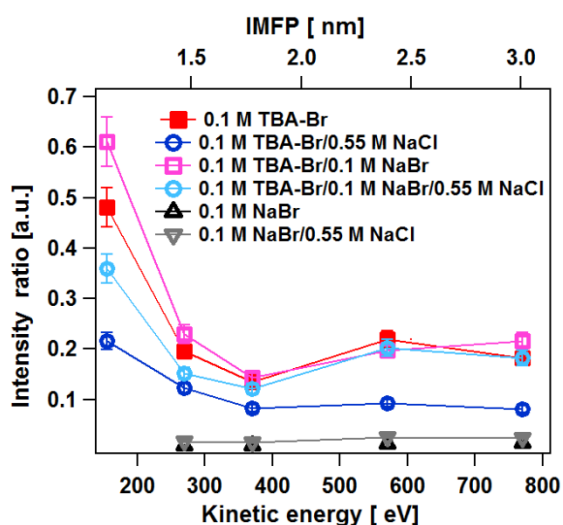


Fig. 1: Br 3d photon emission (PE) signal intensity of various mixed TBA / halide solutions normalized by the condensed phase O 1s PE signal of H₂O, the photon flux, and the cross section as a function of electron kinetic energy.

We acquired Br 3d core level spectra of 0.1 M TBA bromide, 0.1 M TBA-Br / 0.55 M NaCl, 0.1 M TBA-Br / 0.1 M NaBr, 0.1 M TBA-Br / 0.1 M NaBr / 0.55 M NaCl, 0.1 M NaBr, and 0.1 M NaBr / 0.55 M NaCl aqueous solutions. TBA-Br is expected to exhibit a surface excess of $\sim 2.3 \times 10^{14}$ molecule per cm² at 0.1 M [4]. The spectra are normalized to the O 1s PE signal of condensed phase H₂O-oxygen. The probe depth was varied by varying the photoelectron kinetic energy, E_k , and thus inelastic mean free path (IMFP, λ) via variation of the probing photon energy. The photoemission (PE) intensity, I , of a solute can be split into contributions from surface and bulk. When attenuation of photoelectrons

originating from the surface molecules is neglected, the surface contribution is proportional to the surface excess (Γ_X). The bulk contribution is proportional to ($n_{b,X} \times \lambda$), where $n_{b,X}$ is the bulk number density of the solute. Thus the ratio of $I_{Br\ 3d}$ and $I_{O\ 1s}$, the PE signal intensities for the solutions and H₂O of liquid water, respectively, each normalized to photon flux and ionization cross section, is then:

$$\frac{I_{Br\ 3d}}{I_{O\ 1s}} = \frac{(\Gamma_{Br^-} + n_{b,Br^-} \times \lambda)}{n_{b,H_2O} \times \lambda} \quad (\text{eq. 1})$$

In Fig. 1, this ratio decreases with E_k , which means a positive surface excess for bromide in solutions containing TBA, which is also in agreement with the positive surface excess of TBA bromide [4]. This is likely due to ion pairing between bromide anions and the TBA cations. In turn, for the solutions in absence of TBA bromide, the Br signal intensity is much lower and slightly increases with E_k , which indicates a negative surface excess for both, pure NaBr and mixed NaBr/NaCl, which has already been observed elsewhere [5].

In addition, when we focus on the lowest E_k , which corresponds to the most surface sensitive measurement: The Br intensity difference between the TBA bromide and mixed TBA-Br / NaCl may be explained by the possibility that some of the Cl⁻ is replacing Br⁻ in ion pairing with TBA. Further, when additional NaBr is added into the TBA-Br solutions, the Br intensity at the surface increases by $\sim 20\%$, which may be explained the fact that for pure TBA bromide solutions, ion pairing between TBA and bromide is not yet complete at the interface, so that additional bromide leads to even higher density of ion pairs at the interface.

This enhanced bromide concentration in the interfacial region for TBA bromide containing solutions may then be the reason for the enhanced oxidation kinetics by ozone, shown in kinetic experiments in the laboratory for the same system, where a strongly enhanced ozone loss rate in presence of TBA on the surface of bromide solutions was observed.

We acknowledge funding from the Swiss National Science Foundation (Grant 169176).

- [1] S. Wang et al., Proc. Natl. Acad. Sci., **112**, 9281-9286 (2015).
- [2] L. Artiglia et al., Nature. Comm., **8**,700 (2017).
- [3] M. A. Brown et al., Rev. Sci. Instrum, **84**, 073904 (2013).
- [4] J. Mata et al., Coll. Surf. A, **245**, 69-73 (2004).
- [5] N. Ottosson et al., J. El. Spectr. Rel. Phen., **177**, 60-70 (2010).

ICE NUCLEATION ACTIVITY OF FRESH AND AGED PROPANE FLAME SOOT

F. Mahrt, J. Dou, U. Lohmann, Z. A. Kanji (ETHZ), P. A. Alpert, M. Ammann (PSI),
P. Corral Arroyo (PSI & Univ. Bern), P. Grönquist (ETHZ & EMPA)

This work investigates the ice nucleation ability of fresh and aged propane flame particles derived from different combustion conditions, combined with soot particle characterization using spectroscopic techniques and dynamic vapor sorption.

Soot particles are directly emitted to the atmosphere, formed as by-products of incomplete combustion of fossil fuels and biomass. They are carbonaceous and have an important anthropogenic source in addition to natural sources, e.g., biomass burning. Soot can initiate the formation of ice clouds, which affect the global cloud radiative properties, precipitation formation and distribution and ultimately influence climate. Predicting ice nucleation activity of soot is uncertain. Greater ice nuclei concentrations due to soot can either increase or decrease the ice particle number concentration, depending on the conditions, thus affect cloud cover (lifetime) [1]. Soot particle morphology and composition are believed to be key factors in determining the ice nucleation activity of soot [2], and can vary depending on fuel source and combustion conditions [3]. Morphology can also change upon particle ageing [4], further complicating their environmental fate.

We generated propane flame soot from a miniCAST burner with different size and organic content depending on combustion conditions. The soot was aged by submerging soot in water at pH 7 and 4, the latter being in the range of cloud droplets or contrails formed through aviation emission. We use scanning transmission X-ray microscopy with near-edge X-ray absorption fine structure spectroscopy to map chemical functional groups and particle morphology on a single particle level. Our measurements are complemented by quantification of particle hydrophilicity using dynamic vapor sorption.

Fig. 1 shows the fraction of fresh soot and water aged soot particles that can nucleate ice at a temperature of 218 K. Ice nucleation activity of aged soot was observed to be enhanced with respect to non-aged soot. We have found distinct spectral differences between these two samples as illustrated in the X-ray absorption spectra in Fig. 2a. For instance, fresh soot had ketone functions indicated by an absorption peak at 287 eV which was absent for aged soot. Aged soot had a greater absorption peak signature at 285.4 eV attributable to carbon double bonding. We also observed enhanced water uptake by the aged soot shown in Fig. 2b as compared to the fresh sample, which correlated to enhanced ice nucleation ability of aged soot seen in Fig. 1.

Our results indicate that fresh propane flame soot is not a good ice nucleating particle, but that water ageing can chemically change the soot and simultaneously enhance its ice nucleation ability. Ketone functions associated

with freshly generated soot may then need to be stripped off particles to obtain higher activated fractions. This is important for quantifying the chemical properties of atmospheric soot particles, which may strongly influence their ice nucleation activity. We also suggest considering that when soot particles are involved in cloud processing and atmospheric aging, their ice nucleation ability may change.

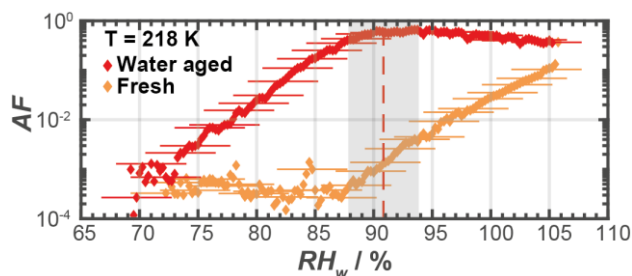


Fig. 1: Ice activated fraction (AF) of soot particles as a function of relative humidity with respect to water (RH_w), for fresh (orange) and water aged (red) propane flame soot with little to no organic content.

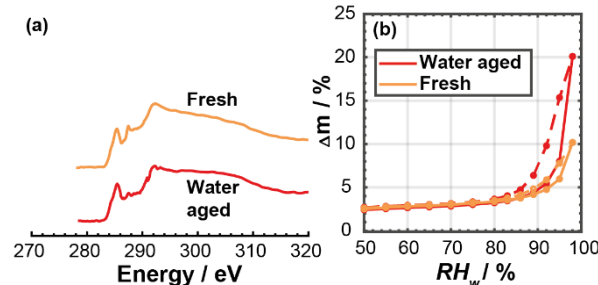


Fig. 2: (a) Example C K-edge X-ray absorption spectra of fresh and water aged soot and (b) particle hydrophilicity, given as water uptake (mass change) as a function of RH_w for adsorption (solid lines) and desorption (dashed), respectively.

We acknowledge funding from the ETH Research Grant (ETH-25-15-1), the FoKo-CROSS project “Scanning transmission X-ray spectro-Microscopy of atmospheric particles and processes: advanced environmental cell development” co-funded by ENE and PSD research divisions at PSI and the European Union’s Horizon 2020 research and innovation programme under the Marie Skłodowska-Curie grant agreement (701647).

- [1] T. C. Bond et al., *JGR – Atmospheres*, **118**, 5380-5552 (2013).
- [2] F. Mahrt et. al., *ACP Physics*, **18**, 13363-13392 (2018).
- [3] S. di Stasio, A. Braun, *Energy & Fuels*, **20**, 187-194 (2006).
- [4] V. Zelenay et al., *ACP*, **11**, 11777-11791 (2011).

WATER STRUCTURE IN PRESENCE OF A SURFACE ACTIVE ORGANIC SOLUTE

H. Yang (PSI & ETHZ), L. Artiglia (PSI LSK & LUC), J. P. Gabathuler (PSI & ETHZ), A. Boucly (PSI), S. Chen (PSI & ETHZ), M. Ammann (PSI)

The oxygen K-edge NEXAFS spectrum of liquid water is sensitive to changes in the local electronic environment experienced by the water molecules [1]. The addition of an organic solute to liquid water engenders such electronic structure changes due to solute – solvent interactions [2].

It has been suggested from theory and mostly non-linear optical spectroscopy experiments [3] that the water structure near ice nucleation active proteins, surfactants and organics is changed towards promoting the formation of tetrahedrally coordinated water clusters. 1,3,5-Trihydroxybenzene (THB) and 1,5-Dihydroxynaphthalene (DiHN) may have the potential to enhance ice nucleation in aqueous solutions and particularly in suspensions [4], therefore they may play a role in heterogeneous ice nucleation in the atmosphere. In this work we have attempted at observing changes in the water structure due to these two solutes by means of electron yield NEXAFS spectra.

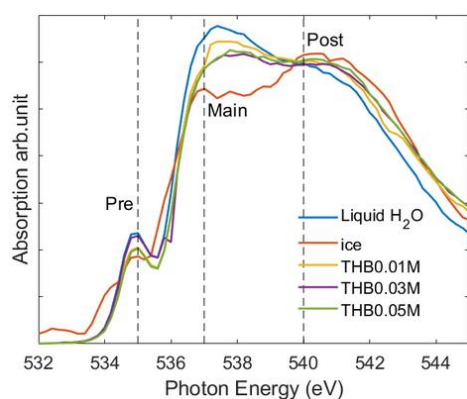


Fig. 1: Electron yield O K-edge NEXAFS spectra of THB solutions at three different concentrations. The liquid water (blue) and ice (red) spectra are also shown for comparison.

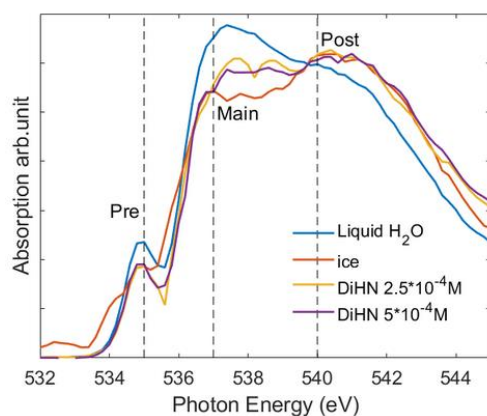


Fig. 2: Electron yield O K-edge NEXAFS spectra of DiHN solutions at two different concentrations. The liquid water (blue) and ice (red) spectra are also shown for comparison.

Liquid water (blue, Fig. 1) consists mainly of water molecules with only one strong donating H bond (donor configuration) [5] and the other H bond is relatively “weak” in terms of energy due to the elongation or bending of the OH--O axis [5,6]. These contribute to the features of the pre- (~535eV) and main (~537eV) edges in the NEXAFS spectrum (Fig. 1). In contrast to liquid water, all water molecules in ice (red, Fig. 1) are highly ordered due to the high population of tetrahedrally coordinated strong H bonds, contributing to a stronger post-edge (~540eV) feature in the spectrum.

In Fig.1 we show oxygen K edge NEXAFS spectra of the THB solutions at 0.01 M, 0.03 M and 0.05 M. In comparison with liquid water, THB solutions show a general decrease in the intensity of the main edge observed at around 537.5 eV with a concomitant increase in the post-edge (~541 eV), which reflects a higher abundance of tetrahedrally coordinated water molecules. Furthermore, as the concentration increases from 0.01 M to 0.03 M, this effect is getting more pronounced. This experimental result indicates that the water molecules near the surface of THB solution are more tetrahedrally coordinated. The effect may be quite pronounced because THB is very surface active, leading to high surface density of the THB related OH functional groups. Whether this effect is related to the ice nucleation activity of THB must remain open for further study.

The oxygen K-edge NEXAFS spectra for 1,5-Dihydroxynaphthalene solutions are shown in Fig. 2. As in the case of THB, the addition of DiHN engenders a decrease in the pre-edge (~535.5 eV) and main edge (~537 eV) features and a strong increase in the post-edge (~541 eV) feature. The effect is even more pronounced than that of THB. Further experiments and analysis need to elucidate whether the difference is due to different surface excess of the two solutes and thus different surface densities of OH groups.

We acknowledge funding from the Swiss National Science Foundation (Grant 169176). We thank T. Koop and V. Molinero for helpful discussions.

- [1] C. D. Cappa et al., *J. of Phys. Chem. B*, **109**, 7046-7052 (2005).
- [2] C. D. Cappa et al., *J. of Phys. Chem. B*, **110**, 1166-1171 (2006).
- [3] B. G. Pummer et al., *Atmos. Chem. Phys.*, **15**, 4077-4091 (2015).
- [4] N. J. Fukuta, *Atmos. Sciences*, **23**, 191-196 (1996).
- [5] P. Wernet et al., *Science*, **304**, 995-999 (2004).
- [6] S. Myneni et al., *J. of Phys.*, **14**, L213 (2002).

THE STRUCTURE OF ADSORBED WATER ON ALKALI FELDSPAR SUBSTRATES

H. Yang (PSI & ETHZ), L. Artiglia (PSI LSK & LUC), A. Boucly, T. Bartels-Rausch (PSI),
J. P. Gabathuler (PSI & ETHZ), M. Ammann (PSI)

We want to provide a more detailed understanding of the fundamental aspects of the interaction of water vapor with solid oxide materials in comparison to their known ice nucleation activity.

Potassium containing feldspars (microcline) have been considered as important mineral dust components for ice nucleation in mixed phase clouds. On the other hand, sodium-rich feldspar is believed to have contrasting ice nucleation ability [1]. Hence, for the adsorbed interfacial water layer on the surface, we expect a different hydrogen bonding structure under subsaturated conditions with respect to ice, which is related to the interactions between water molecules and the surface structure of the feldspars.

Electron yield near edge X-ray absorption fine structure (NEXAFS) spectroscopy at the oxygen K-edge is used to experimentally explore the difference between the hydrogen bonding structure of H₂O molecules under different physical conditions. Experiments reported in this work were performed at the *in situ* electron spectroscopy endstation at the NANOXAS beamline at the Swiss Light Source (PSI, SLS).

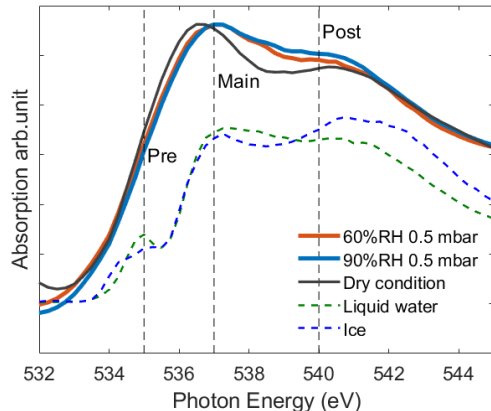


Fig. 1: Electron yield O K-edge NEXAFS spectra from microcline at dry condition (solid black), in presence of water vapour at 0.5 mbar at a relative humidity of 60% at -22°C (solid red) and 90% at -25°C (solid blue). Spectra from liquid water (dashed green) and solid ice (dashed blue) are shown for comparison. Pre-edge (~535eV), main edge (~537eV) and post-edge (~540eV) are indicated by black vertical dashed lines.

Liquid water (dashed green, Fig 1) consists mainly of water molecules with only one strong donating H bond as described on the previous page [2, 3]. These contribute to the features of the pre and main edges in the NEXAFS spectrum (Fig. 1). In contrast to liquid water, all water molecules in ice (dashed blue, Fig 1) are highly ordered due to the high population of tetrahedrally coordinated strong H bonds, contributing to a stronger post-edge feature in the spectrum (Fig. 1).

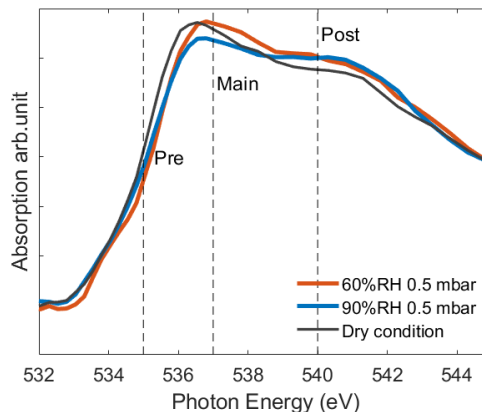


Fig. 2: Electron yield O K-edge NEXAFS spectra from microcline at dry condition (solid black), in presence of water vapour at 0.5 mbar at a relative humidity of 60% at -22°C (solid red) and 90% at -25°C (solid blue).

In Fig.1 we show the electron yield O K-edge NEXAFS spectra from microcline at dry condition, 60% and 90% RH; spectra were normalized to unity within the energy range from 532 to 545 eV. Compared to dry conditions, the main edge of the microcline spectrum in presence of water vapor is shifted by about 0.5eV towards higher energy, which arises from the difference between lattice oxygen and water oxygen. As the RH increases, an increase in post-edge intensity is observed, indicating an increase in highly ordered structures of the hydrogen bonding network of water molecules, while the main edge of the spectra remains the same. On the other hand, in Fig.2, the albite shows a different spectral evolution from RH 60% to 90%, the main edge is getting lower, while the post-edge remains the same, indicating an increase in the fraction of ice-like water at higher RH. Linear decomposition (not shown) of these spectra at 90% RH shows that the microcline surface features a larger fraction of liquid-like water than albite in presence of water vapor, although they show a comparable amount of ice-like contribution. Future analysis will consist of deconvoluting the spectra into several Gaussian peaks in order to better fit the transient cases between ice and liquid like spectra and relate the conclusions about the structural changes with literature reports about the ice nucleation ability of microcline and albite and corresponding theoretical studies.

We acknowledge funding from the Swiss National Science Foundation (Grant 169176).

- [1] A. D. Harrison et al., *Atmos. Chem. Phys.*, **16**, 10927-10940 (2016).
- [2] P. Wernet et al., *Science*, **304**, 995-999 (2004).
- [3] S. Myneni et al., *J. Phys.*, **14**, L213 (2002).

LIQUID LIKE LAYER (LLL) IN THE SPOTLIGHT

J. P. Gabathuler, H. Yang (PSI & ETHZ), L. Artiglia (PSI LSK & LUC), A. Boucly, M. Ammann, T. Bartels-Rausch (PSI)

As temperature increases towards the melting point of ice, disorder of the hydrogen-bonding network at the interface with the gas phase increases, creating what is known as the Liquid Like Layer (LLL). We take advantage of the surface-sensitivity of electron spectroscopy to shed light on this LLL.

Near Edge Absorption Fine Structure spectroscopy (NEXAFS) is an experimental technique to visualize the energy states and hybridization of molecular orbitals and therefore, such measurement allows distinguishing water in its solid, liquid and gas phase state. If based on the detection of electrons, NEXAFS is highly sensitive to the surface region of a few nanometer depth [1].

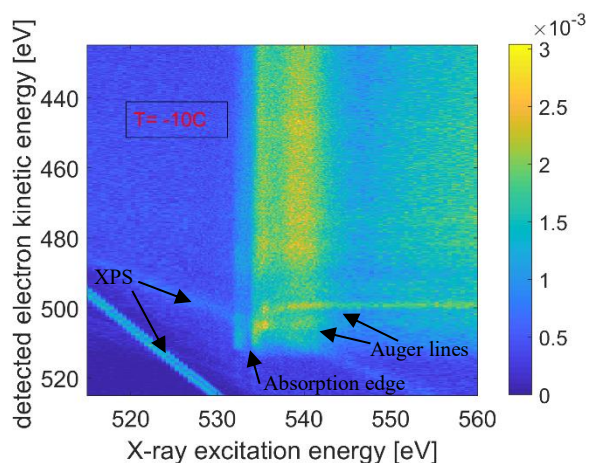


Fig. 1: Data image of a O K-edge NEXAFS measurement of ice at -10°C . One can see XPS peaks traveling in the bottom left corner, Auger lines (horizontal), main and post-edge.

Fig. 1 shows a typical O K-edge NEXAFS image where the intensity (color scale) of detected electrons is plotted as a function of the X-ray excitation energy (x-axis) and of the kinetic energy (y-axis). The main feature of interest is the emission of Auger electrons setting in at 532 eV excitation energy due to excitation from the O 1s orbital to the lowermost unoccupied molecular orbitals (LUMO). From this data image, several processing steps are required to extract a NEXAFS spectrum as shown in Fig. 2. The NEXAFS spectrum shows the summed intensity of Auger emission versus excitation energy. First, fluctuations in X-ray intensity with excitation energy need to be treated. Indeed, the photon energy striking the sample is modulated by X-ray absorption by species adsorbed on beamline components. Second, one typically subtracts the background, i.e. the region before 528 eV, by a linear approximation. Finally, it is convenient to normalize the obtained spectra to their integrated area between 535 eV and 540 eV for explicit comparison.

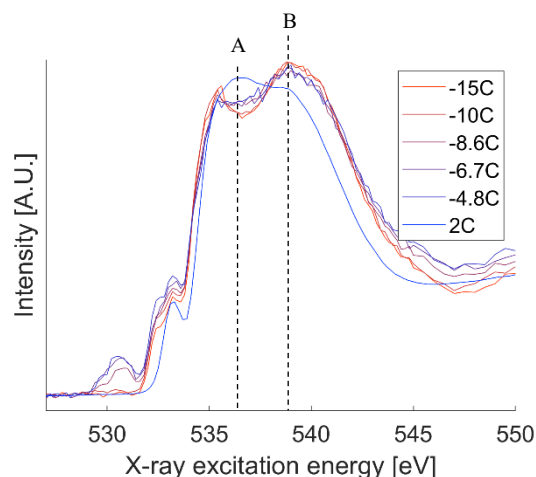


Fig. 2: NEXAFS spectra of pure ice acquired at the NanoXAS beamline showing differences in regions A and B as temperature is increased towards the melting point. Peaks at 530 eV indicate carbon contamination. NEXAFS spectra of water acquired at the SIM beamline are also shown for comparison.

Strikingly, these early results presented in Fig. 2 reveal very little change of the NEXAFS spectra, and thus the hydrogen-bonding network, as temperature increases [2]. Cold ice appears to have a slightly more pronounced dip (region A) and a stronger signal in region B compared to warmer ice. This suggests, when comparing with liquid water spectra, that the LLL thickness is contributing not more than 10% to the total signal, which correspond to a ~ 0.3 nm thickness difference from -15°C to -5°C . Currently, we cannot exclude that the carbon contamination, which was higher during the measurement of warmer ice spectra, impacted the LLL thickness. Future measurement and detailed analysis of the data will tackle this issue.

We acknowledge funding from the Swiss National Science Foundation (Grant 178962). We thank the staff of NanoXAS for their support, and A. Laso for technical help.

- [1] M. Ammann et al., “X-Ray Excited Electron Spectroscopy to Study Gas-Liquid Interfaces of Atmospheric Relevance”, chapter in: “Physical Chemistry of Gas-Liquid Interfaces” (J. A. Faust, J. E. House, eds.), Elsevier (2018).
- [2] T. Bartels-Rausch et al., *Atmos. Chem. Phys.*, **14**, 1587-1633 (2014).

CHEMICAL REACTIVITY DURING SNOW METAMORPHISM

J. Edebeli (PSI & ETHZ), S. E. Avak (PSI & Univ. Bern), J. Trachsel (WSL-SLF & ETHZ), M. Schneebeli (WSL-SLF), A. Eichler, M. Ammann, T. Bartels-Rausch (PSI)

We observed that snow metamorphism may lead to incorporation of bromide in the bulk of snow grains, thereby decreasing bromide availability for reaction and increasing bromide preservation.

Dry metamorphism in snow involves the flux of water vapor across a vapor pressure gradient; this results in restructuring with up to 60% mass turnover [1]. This study investigates whether ions trapped in snow are redistributed with the movement of water vapor in the snowpack by observing the change in the uptake of ozone (O_3) in bromide (Br^-) doped snow after 12 days under temperature gradient induced metamorphism (TGM).

Artificial snow produced from shock frozen droplets of ultrapure water (18 M Ω ; clean) and 6 μ M NaBr solution (doped) in liquid nitrogen were exposed to a temperature gradient of 33 Km $^{-1}$ for 0 and 12 days. Before exposure to TGM, all samples were stored at -5°C for 7 days to decrease grain boundaries [2]. The structural changes in the snow samples were obtained using X-ray computer micro-tomography (Scanco micro-CT, 10 μ m resolution) at -20°C . O_3 uptake was observed by exposing the samples in a flow reactor setup to O_3 at 7 cm 3 s $^{-1}$ at -15°C in the dark. O_3 uptake coefficients in the snow were calculated using the following eqn:

$$\gamma_{obs} = 4\phi \ln([O_3]_{bypass}/[O_3]_{flowtube})/(\omega_{O_3} \times TSA)$$

Where γ_{obs} is the observed uptake coefficient, ϕ is the gas flow rate, ω_{O_3} is the mean thermal velocity of O_3 , and TSA is the total surface area (SSA (cm 2 g $^{-1}$) \times mass of snow (g)).

Table 1: Structural properties of the snow samples; TGM age is days exposed to the temperature gradient. SSA is specific surface area ($\pm 6\%$ error; [3]). ϵ is porosity, K , permeability [4].

TGM age	Sample	SSA cm 2 g $^{-1}$	ϵ	K m 2
0	Clean (<10 ppbv)	176 \pm 11	0.45 \pm 0.005	1.6 \pm 0.43 $\times 10^{-10}$
12	Clean (<10 ppbv)	167 \pm 10	0.56 \pm 0.01	6.0 \pm 1.45 $\times 10^{-10}$
0	Doped (498 ppbv)	183 \pm 11	0.47 \pm 0.01	1.8 \pm 0.49 $\times 10^{-10}$
12	Doped (498 ppbv)	162 \pm 10	0.47 \pm 0.001	2.3 \pm 0.57 $\times 10^{-10}$

There was a decrease in the γ_{obs} after 12 days under TGM (Fig. 1). At the same time, there was no significant difference in the structural properties between 0 and 12 days under TGM for the clean and doped samples (Table 1). The decrease in γ_{obs} is therefore an indication of reduced availability of Br^- for reaction on the exposed surfaces of the snow grains after 12 days under TGM and rather not caused by structural changes. This is in agreement with other studies, which indicate that bromide may be incorporated in the bulk of snow grains over time [5].

This result has potential implications for the ice core community and for polar atmospheric chemistry. With decreased availability of Br^- for reaction, there is a potential for its increased preservation in ice; there are studies already applying Br^- as a tracer in ice cores [6]. This also implies that, with time, Br^- will be less available for oxidation due to dry metamorphism; hence, a reduction in reactive bromine production.

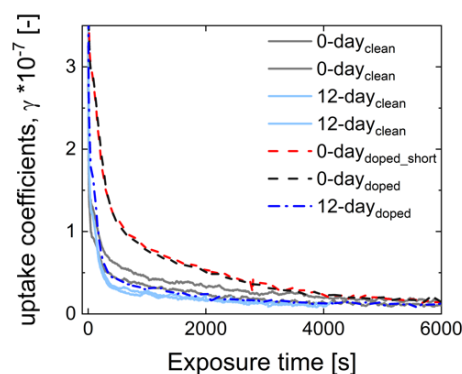


Fig. 1: O_3 γ_{obs} as a function of exposure time to O_3 at -15°C (for all experiments, O_3 concentration was 163 to 190 ppb; maximum variation in any one experiment < 5 ppb).

We acknowledge funding from the Swiss National Science Foundation (Grant 155999).

- [1] B. R. Pinzer et al., *Geophys. Res. Lett.*, **36**, (2009).
- [2] F. Riche et al., *J. Glaciol.*, **58**, 815-817 (2012).
- [3] M. Kerbrat et al., *Atmos. Chem. Phys.*, **8**, 1261-1275 (2008).
- [4] N. Calonne et al., *The Cryosphere*, **6**, 939-951 (2012).
- [5] E. R. Davis et al., *Biogeochemistry of seasonally snow-covered catchments (proceedings of a Boulder Symposium)*, **228**, 115-126 (1995).
- [6] A. Spolaor et al., *Sci. Rep.*, **6**, 33925 (2016).

BIOMASS BURNING IN THE AMAZON BASIN RECORDED IN ILLIMANI ICE CORE

D. Osmont (PSI & Univ. Bern), M. Sigl, A. Eichler, T. M. Jenk (PSI), M. Schwikowski (PSI & Univ. Bern)

We present the first Andean black carbon ice-core record, obtained from Illimani glacier and spanning the entire Holocene, and connect it to biomass burning activity in the Amazon Basin.

The Amazon Basin is one of the major contributors to global biomass burning emissions. However, regional paleofire trends remain partially unknown. Due to their proximity to the Amazon Basin, Andean ice cores are suitable to reconstruct paleofire trends in South America and improve our understanding of the complex linkages between fires, climate and humans.

Here we present the first black carbon (BC) ice-core record from the Andes as a proxy for biomass burning emissions in the Amazon Basin, derived from an ice core drilled at 6300 m from Illimani glacier in the Bolivian Andes and spanning the entire Holocene (last 13000 years). At this site, in the Eastern Andes, moisture mainly originates from the Amazon Basin (and ultimately the Atlantic Ocean) [1]. The entire ice core was cut into 3070 samples which were analyzed at PSI for BC with a Single Particle Soot Photometer (SP2).

To investigate major causes for BC changes during the 20th century, we studied spatial and temporal correlations between the Illimani BC record and two important drivers of biomass burning activity, namely temperature and precipitation. Significant spatial correlations ($p < 0.05$) between the BC record and re-analyzed temperature and precipitation from the NCEP/NCAR R1 dataset were found for areas in the Amazon Basin east of the Illimani site (Eastern Bolivia, Western Brazil and along the arc of deforestation), where extensive fires occur during the dry season (Fig. 1). Comparisons between temperature/precipitation time series for the Amazon Basin (region between 4°N-16°S and 76°W-51°W) and the Illimani BC record confirm that higher BC concentrations were observed during warmer and drier periods, such as the 1900s, the 1940s and the 1960s.

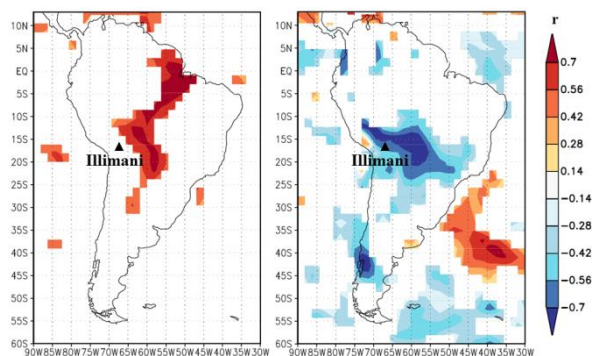


Fig. 1: Spatial correlation over South America between the Illimani BC record and reanalyzed temperature (left) and precipitation (right) from the NCEP/NCAR R1 dataset for the time period 1948–1998.

In the last millennium, a very good agreement is visible between the BC record and reconstructed temperature from the same ice core (Fig. 2a). Higher BC concentrations were observed between 1000 and 1300 AD, corresponding to the Medieval Warm Period (MWP). BC concentrations subsequently declined until they reached a minimum in the 18th century, reflecting the Little Ice Age (LIA). Then, BC concentrations started to rise until present time, at a comparable rate to temperature, suggesting that industrial emissions did not play a significant role there.

The relationship between BC concentrations and regional temperature/moisture variations extends further back in time through the entire Holocene (Fig. 2b). The bottommost part of the ice core shows low BC concentrations, indicative of a cold and wet climate corresponding to last deglaciation conditions. The highest BC concentrations of the entire record occurred during the Holocene Climatic Optimum (HCO) between 7000 and 3000 BC, suggesting that this outstanding warm and dry period caused an exceptional biomass burning activity, unprecedented in the context of the past 13000 years.

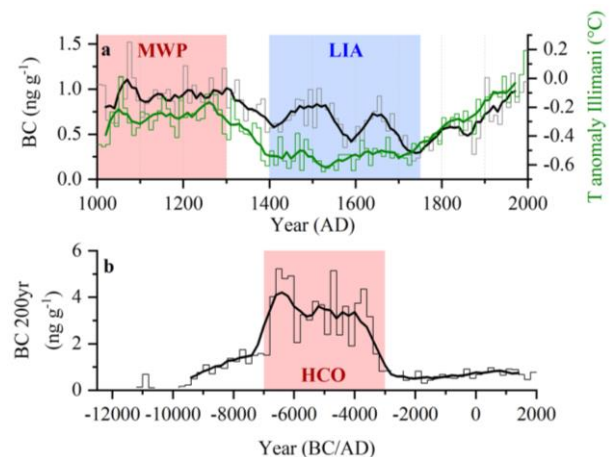


Fig. 2: (a) Illimani BC record of the last 1000 years (left scale) compared to reconstructed temperature from Illimani (right scale, [1]), 10-year averages with 5-pt moving averages. (b) Full BC record from Illimani, 200-year averages with 5-pt moving averages.

We acknowledge funding from the Swiss National Science Foundation (Sinergia: Paleo fires from high-alpine ice cores 154450).

- [1] T. Kellerhals et al., *J. Geophys. Res.*, **115**, D16123 (2010).

6000 YEARS OF FIRE DYNAMICS FROM AN ALTAI ICE CORE

D. Osmont (PSI & Univ. Bern), M. Sigl (PSI), M. Schwikowski (PSI & Univ. Bern)

The black carbon record from the Tsambagarav ice core, Mongolian Altai, is used to reconstruct fire dynamics in this region, revealing a much higher fire activity in the oldest 1000 years of the core in the context of a predominant Monsoon regime. Recent industrial pollution from the former USSR is also visible between 1960 and 1990.

The Mongolian Altai, located between the Siberian taiga belt (north) and the Gobi desert (south), is the region with the highest degree of continentality in the world and has been strongly affected by recent climate change [1]. In this steppe region, fire is an important element regulating the ecosystem. To predict future fire evolution in a changing climate, knowledge of past fire dynamics is needed. However, in this remote region, paleofire records are scarce [2]. Here, we present the black carbon (BC) record from the Tsambagarav ice core, Mongolia, as a proxy for paleofire activity. This ice core, extracted in 2009 from the Khukh Nuru Uul ice cap at 4130 m a.s.l. was shown to span the last 6800 years [1]. 2448 samples were analyzed for BC using a Single Particle Soot Photometer (SP2).

A much larger variability was observed in the oldest 1000 years of the BC record compared to the following 5000 years (Fig. 1), in the context of more humid conditions. The latitudinal position of the Intertropical Convergence Zone (ITCZ) was suggested to influence this variability. Greater variability was associated with a predominant Monsoon regime during the Holocene Climatic Optimum (HCO), when the ITCZ was located further north, which then shifted to a more stable and drier climate regime dominated by Westerlies towards the late Holocene. Interestingly, in this region, wetter conditions seem to promote fire activity because they enhance grassland productivity and therefore increase the amount of available fuel.

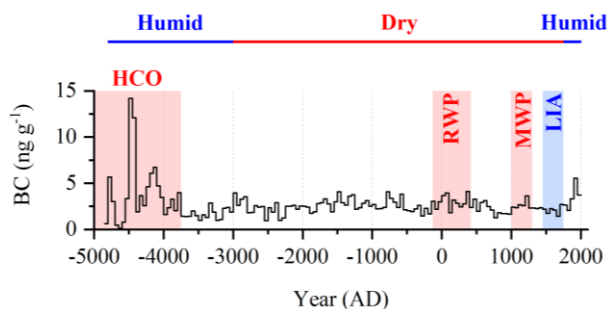


Fig. 1: The entire BC record from the Tsambagarav ice core (50-year averages).

In the following 5000 years, little variations were visible in the BC record. The Roman Warm Period (RWP), Medieval Warm Period (MWP) and Little Ice Age

(LIA) were barely visible, except a local minimum during the colder period of the Maunder solar minimum. A weak correlation was found between BC and ammonium, suggesting that the latter originate from a different source, namely biogenic emissions.

In the 20th century, BC background concentrations reached unprecedented levels since the HCO. They peaked in the 1970s and 1980s and subsequently strongly declined in the 1990s (Fig. 2a). A similar pattern was observed for sulfate, a well-known tracer for fossil fuel burning emissions (Fig. 2b). This feature reflects industrial BC emissions from the former Soviet Union and is well reproduced by BC emission inventories (Fig. 2c, [3]). The sharp decline in the 1990s can be explained by the USSR collapse and the sudden drop of many heavy industries.

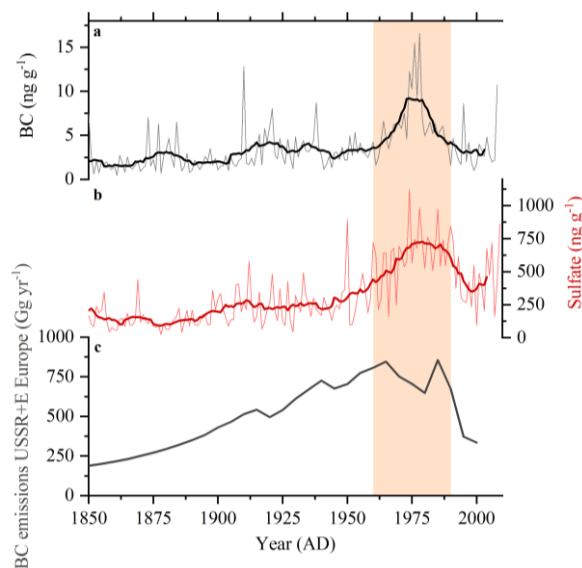


Fig. 2: Time period 1850–2009 AD: (a) BC and (b) sulfate records from Tsambagarav. Thin lines: annual averages, thick lines: 11-year moving averages. (c) Industrial BC emission estimates for Eastern Europe and former USSR countries at 5-year resolution [3]. Orange bar: maximum of emissions, 1960–1990 AD.

We acknowledge funding from the Swiss National Science Foundation (Sinergia: Paleo fires from high-alpine ice cores 154450).

- [1] P.-A. Herren et al., *Quaternary Sci. Rev.*, **69**, (2013).
- [2] S. O. Brügger et al., *Global Planet. Change*, **169**, (2018).
- [3] T. C. Bond et al., *Global Biogeochem. Cy.*, **21**, (2007).

ICE RECORDS REVEAL REGIONAL FOSSIL FUEL POLLUTION

*S. O. Brügger, E. Gobet (Univ. Bern), M. Sigl (PSI), T. Blunier (Univ. Copenhagen),
M. Schwikowski (PSI & Univ. Bern), W. Tinner (Univ. Bern)*

We reconstruct long-term atmospheric pollution trends deriving from fossil fuel burning based on continuous optical analyses of spheroidal carbonaceous particles (SCPs) in globally distributed ice cores.

SCPs are a byproduct emitted to the atmosphere during incomplete combustion of fossil fuels (coal or petroleum products) at high temperatures [1]. They are transported over long distances and deposited in natural archives that preserve them over centuries. Previous compilations of SCP records from lake sediments suggest that the deposition of SCPs in lake sediments usually starts after 1850 AD and that SCP concentrations increase rapidly post-1950 AD. This SCP rise was proposed as a globally synchronous stratigraphic marker for growing human impact suitable to delineate the onset of the new geological epoch “Anthropocene” [1].

Ice records provide excellent chronologies, especially for the most recent 200 years, where they rely on annual layer counting and absolute time markers [2]. We use microscopy to identify SCP >10 μm in globally distributed ice archives covering a large range from highly industrialized to extremely remote regions (Fig. 1). Our ice cores derive from Colle Gnifetti in the Swiss Alps [2], Tsambagarav in the Mongolian Altai [3], Illimani in the Bolivian Andes [4], and Summit in Central Greenland [5].

Our ice records suggest that in Eurasia detectable amounts of SCP accumulated in the ice already during the 18th century (i.e. Colle Gnifetti and Tsambagarav ice records, Fig. 1). Although the first appearance of SCP is unexpectedly early compared to lake sediments, it is corroborated by historical sources in both regions. In the Altai region, the historical onset of larger-scale smelting dates to 1729 AD, which coincides with the beginning of the SCP-derived pollution signal in our Mongolian ice record around 1720 AD [3]. The first SCP in the Colle Gnifetti record appear around 1770 AD. While on the European mainland timber remained the main energy supplier until the 19th century, historical sources document massive coal consumption in Great Britain (e.g. >650,000 tons of black coal were shipped each year [6]). The onset of SCP in the Andean ice core dates to 1820 AD and coincides with the independence from the Spanish viceroyalty (1809–1825 AD) and a growing exchange with English coal-experienced mariners that initiated the use of black coal [7]. Astonishingly, atmospheric fossil fuel pollution including rather large particles (i.e. ca. 10 μm) reached even the remote Greenland site around 1900 AD, coinciding with the start of large-scale Arctic mining activities. While new regulations and associated technical advances strongly reduced atmospheric fossil fuel pollu-

tion in Europe after the 1970s, the increase of SCP concentrations in the ice cores from Central Asia and South America continued during the past decades.

The spatial and temporal heterogeneities of SCP-inferred atmospheric pollution in ice cores across the investigated regions question the use of SCP onset and/or maximum peaks as additional dating horizons in natural archives [1].

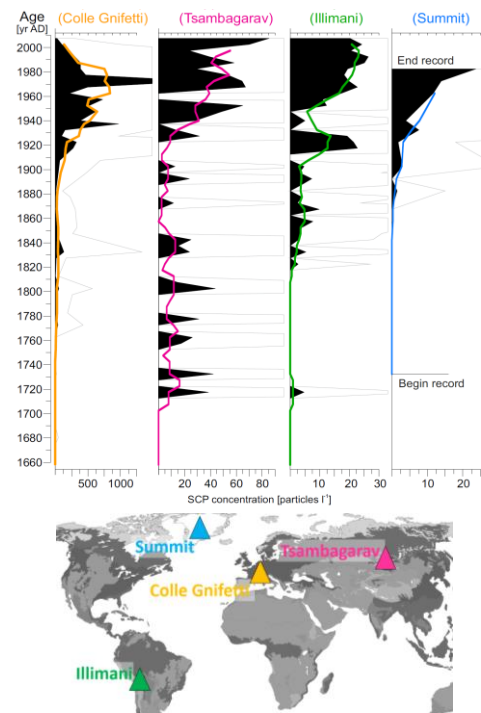


Fig. 1: SCP concentration in ice records 1660 AD–present. X-axes are adjusted to the maximum SCP concentration peak in each record. Hollow curves: 10x exaggeration, colored curves: moving average (period = 5).

We acknowledge funding from the Swiss National Science Foundation (SNF Sinergia Grant 154450).

- [1] N. L. Rose, *Environ. Sci. Technol.*, **7**, 4155–4162 (2015).
- [2] M. Sigl et al., *J. Glaciol.*, **194**, 985–996 (2009).
- [3] P. A. Herren et al., *Quat. Sci. Rev.*, **69**, 59–68 (2013).
- [4] T. Kellerhals et al., *Environ. Sci. Technol.*, **3**, 888–893 (2010).
- [5] T. Blunier et al., *Geophys. Res. Lett.*, **20**, 2219–2222 (1993).
- [6] E. A. Wrigley, *Philos. T. R. Soc. A*, **371** (2013).
- [7] L. M. De Grazia, *Rev. Atenea*, 475–1957 (1997).

MELT-INDUCED FRACTIONATION OF TRACE ELEMENTS IN ALPINE SNOW

S. E. Avak (PSI & Univ. Bern), J. Trachsel (WSL-SLF & ETHZ), J. Edebeli (PSI & ETHZ), S. Brüttsch, T. Bartels-Rausch (PSI), M. Schneebeli (WSL-SLF), M. Schwikowski (PSI & Univ. Bern), A. Eichler (PSI)

Snow pack measurements of trace elements at Weissfluhjoch, Swiss Alps, suggest a well preserved atmospheric composition in winter. Melting in spring causes preferential elution of certain trace elements from the snow pack. Rare-earth and trace elements occurring in low concentrations tend to be most persistent against meltwater-induced relocation.

In collaboration with the WSL-Institute for Snow and Avalanche Research (SLF), the impact of melting on the preservation of atmospheric impurities in snow was studied by conducting an extensive snow pit campaign at the Weissfluhjoch field site, Switzerland. Regular samplings took place from January to June 2017 to monitor the behaviour of trace elements (TEs), an important class of paleo atmospheric reconstruction proxies, during melting of the snow pack (Fig. 1).



Fig. 1: High-Alpine snow is very sensitive to contamination due to the low concentrations of atmospheric TEs. Therefore, special precautions, such as wearing clean room overalls, facemasks, and ultra-clean plastic gloves, were taken during the snow pit samplings.

Snow pit profiles representing dry conditions (insignificant occurrence of melting on Jan 25th, Feb 22nd, and Mar 21st 2017) and profiles representing wet conditions (wet snow pack on Jun 1st 2017) were compared by calculating a concentration ratio $c_{\text{wet}}/c_{\text{dry}}$. c_{wet} represents the average TE concentration of the wet profile and c_{dry} the average TE concentration during dry conditions. This ratio revealed a preferential loss of certain trace elements (Fig. 2), depending on their presumed microscopic location and their water solubility [1]. The obtained elution behaviour matched the findings from the upper Grenzgletscher ice core [1]. Variable mobility was observed for water-soluble TEs originating from partially water-soluble particles, with the low abundant ones preferably retained due to incorporation into the ice interiors. Concentration-independent preservation was visible for water-insoluble TEs. Even though most likely located on ice surfaces, they remained relatively

immobile with meltwater due to their water insolubility. Precipitation at the two 180 km distant high-Alpine sites upper Grenzgletscher and Weissfluhjoch is characteristic for Central European atmospheric aerosol composition. As the large majority of investigated TEs revealed a consistent behaviour with meltwater percolation at those two sites, the proposed applicability of the TEs Ag, Al, Bi, Cu, Cs, Fe, Li, Mo, Pb, Rb, Sb, Th, Tl, U, V, W, Zr, and the rare-earth elements as reconstruction proxies in melt-affected ice core and snow pit records [1] is therefore most likely representative for the entire Alpine region.

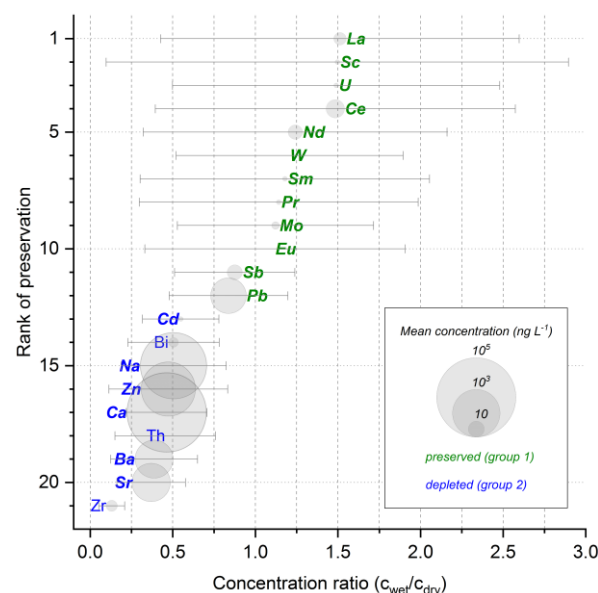


Fig. 2: Rank of preservation plotted against the concentration ratio $c_{\text{wet}}/c_{\text{dry}}$ for each TE classified into group 1 (retained concentration profile) or 2 (depleted concentration profile). Symbols in bold indicate a similar behaviour as observed after meltwater percolation in the firm part of a high-Alpine ice core [2,3]. Circle sizes represent the mean concentrations in the dry snow pits where insignificant melting occurred.

We acknowledge funding from the Swiss National Science Foundation (Grant 155999).

[1] S. E. Avak et al., *J. Glaciol.*, **64**, 877-886 (2018).

A NEW METHOD FOR *IN SITU* ANALYSIS OF TRACE ELEMENTS IN GLACIER ICE

S. E. Avak (PSI & Univ. Bern), M. Guillong, O. Laurent (ETHZ), T. Bartels-Rausch (PSI),
M. Schwikowski (PSI & Univ. Bern), A. Eichler (PSI)

The spatial distribution of trace elements at a grain scale in high-Alpine glacier ice was investigated using a recently developed method. Preliminary results show that the trace element distribution is not correlated with the grain boundary network in sections where high impurity abundance prevails.

Ice core trace element (TE) records from high-Alpine glaciers are invaluable archives to reconstruct past atmospheric pollution. Concentration records of an ice core from upper Grenzgletscher (GG), Switzerland, revealed a fractionation of TEs in a section affected by meltwater percolation [1]. While some TEs suffered significant concentration depletion, others were well preserved. This is most likely the result of TE location at the grain scale and the selective mobilization of TEs during meltwater percolation. Water-insoluble TEs tend to be enriched at grain surfaces, but were mostly preserved because of their immobility with meltwater. Water-soluble TEs were incorporated into the ice lattice depending on their concentration.

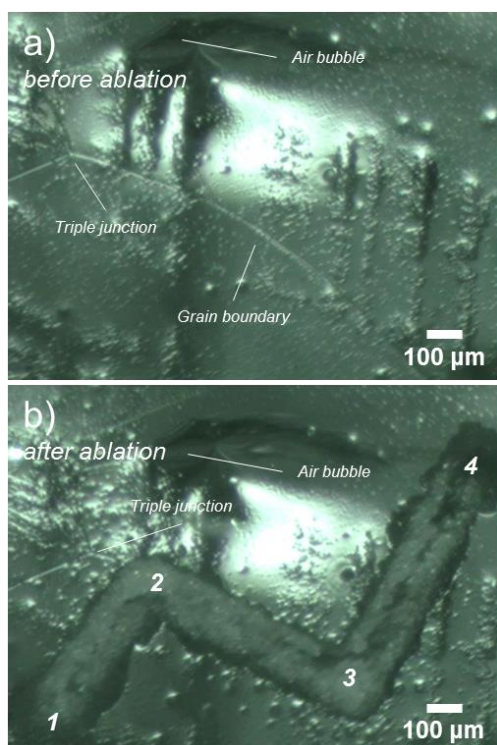


Fig. 1: (a) Surface of the GG sample chosen for cryocell LA-ICP-MS analysis. Three grain boundaries joining a triple junction are visible. (b) Same surface area after LA using a spot size of 163 μm . The sections of the ablation path from 1 to 2, and 3 to 4 are within the grain matrix whereas the path section between 2 and 3 follows a grain boundary.

To be able to corroborate this indirect assessment of TE location in high-Alpine glacier ice, a method based on cryocell laser ablation inductively coupled plasma mass spectrometry (LA-ICP-MS) was recently developed. This technique allows the direct *in situ* analysis of TEs at a sub-millimeter resolution. First measurements of impurity enriched GG samples included ablations of both grain interior and grain boundary material to directly identify differences in TE signal intensities between those two features (Fig. 1). Our results indicate that ice sections exhibiting overwhelming mineral dust abundance do not provide evidence for a linkage between the micro-scale distribution of TEs and the grain boundary network (Fig. 2). Such a dispersion of atmospheric impurities in the ice matrix has also very recently been reported for layers with high impurity enrichment in deep ice from Antarctica and Greenland [2,3,4]. The proposed enrichment of certain TEs at grain boundaries or in grain interiors is most likely present in low concentrations ranges, while TEs seem to be evenly distributed if concentrations are elevated.

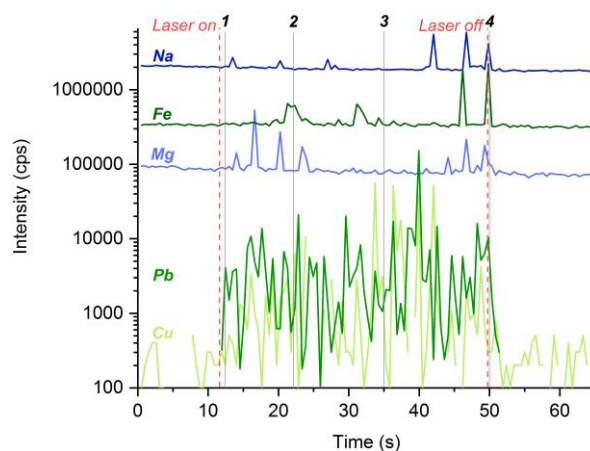


Fig. 2: ICP-MS signal corresponding to the ablation of the GG sample shown in Fig. 1. The time intervals from 1 to 2 and 3 to 4 correspond to the signal acquired within the grain matrix whereas the interval between 2 and 3 reflects the signal of an ablation along a grain boundary.

We acknowledge funding from the Swiss National Science Foundation (Grant 155999).

- [1] S. E. Avak et al., *J. Glaciol.*, **64**, 877-886 (2018).
- [2] J. Eichler et al., *Cryosphere*, **11**, 1075-1090 (2017).
- [3] D. Della Lunga et al., *J. Glaciol.*, **60**, 970-988 (2014).
- [4] D. Della Lunga et al., *Cryosphere*, **11**, 1297-1309 (2017).

TRACE ELEMENT ANALYSIS OF AN ANDEAN ICE CORE USING ICP-TOF-MS

*J. Stegmaier (PSI & Univ. Bern), T. M. Jenk (PSI), T. Erhardt, H. Fischer (KUP, Univ. Bern),
A. Rivera (CECS), M. Schwikowski (PSI & Univ. Bern)*

Ice core trace element (TE) concentrations determined with two mass spectrometric methods (ICP-SF-MS, ICP-TOF-MS) showed similar variability, but significantly different absolute concentrations for TEs present as particles. We attribute this to a size dependent fractionation of particles by the inlet system. Acidification shortly before analysis did not have a significant effect on TE concentrations.

TEs are emitted to the atmosphere from both natural and anthropogenic sources mainly in particulate form [1] and can subsequently be eolian transported until eventually deposited and archived in glaciers. Here, we present first TE analysis results from a 7 m long ice core from the Cerro Negro glacier (4604 m a.s.l.), located in the Chilean Andes in close vicinity of an open-pit copper mine. Measurements were performed using both a conventional ICP-SF-MS (Element2, Thermo Scientific) and a new ICP-TOF-MS (icpTOF, Tofwerk) in order to compare both methods and to finally evaluate the impact of proximal mining activities on TE deposition. The ice core sections were decontaminated by removing the outermost layers and discrete samples were cut with 5 cm resolution using a band-saw in a -20°C cold room. Samples were then transferred into pre-cleaned PP vials and subsequently measured for major ions and black carbon by ion chromatography and incandescence laser spectroscopy, respectively. Afterwards, the leftover sample aliquots were pooled for analysis by mass spectrometry (MS), leading to 40 samples with an approximate resolution of 10 cm. A fraction of 16 samples was then used for final analysis by ICP-TOF-MS at the University of Bern (KUP). Further splitting each of those fractions allowed for analysis without and with prior acidification to 0.2 M HNO₃. All 40 samples were then analysed by ICP-SF-MS at PSI also applying this acidification procedure.

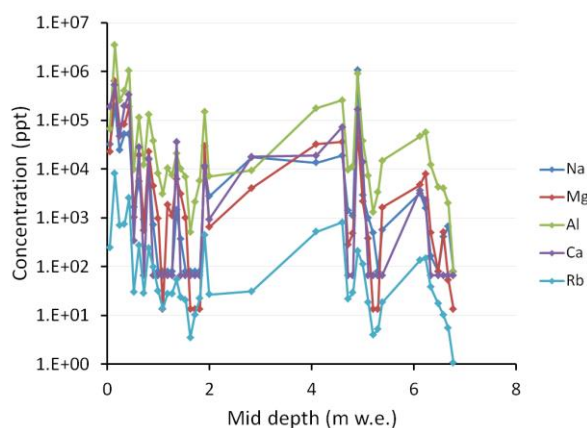


Fig. 1: TE concentrations (ICP-SF-MS) vs. depth in meter water equivalent (m w.e.).

Resulting concentrations are highest in the uppermost part of the ice core (Fig. 1) and at a depth of around 5 m w.e. for all elements. Highest abundances were obtained for typical mineral dust tracers such as Al, Mg, Na, Ca and Rb, whereas elevated concentrations of Cu, Ba and Mn, might reflect the influence of proximal mining activities.

Comparing TE concentrations measured with and without addition of HNO₃ prior to analysis showed that the effect of acidification is negligible for such short time of leaching for all investigated elements.

Applying the single particle measurement mode of the icpTOF (time resolution of 2 ms) results in mass spectra, where single particles create sharp peaks above the dissolved background. This indicates that Al is mostly present in particles, whereas Na, Mg and Ca prevail in dissolved form. Mn, Cu and Ba show elevated background concentrations with few distinct and coinciding particle peaks, suggesting a common emission source.

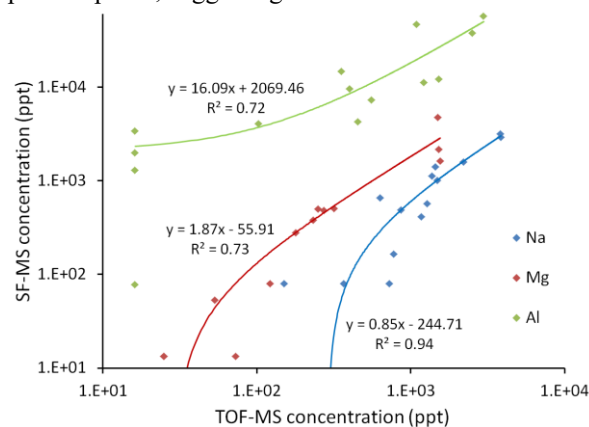


Fig. 2: Concentrations of Al, Na and Mg obtained by ICP-SF-MS and ICP-TOF-MS, respectively.

While general TE variations are similarly reflected by both methods, absolute concentrations vary significantly for some elements (i.e. high R² but slopes ≠ 1, Fig. 2). TEs such as Na and Mg, which are predominantly in dissolved form show good agreement in absolute concentrations, whereas concentrations of Al, Rb, Ba, Nd and Pb were significantly higher if measured by ICP-SF-MS compared to the ICP-TOF-MS. This might be due to the different inlet systems (e.g. spray chamber) of the two MS, which behave differently in terms of size dependent fractionation of the particles introduced into the plasma, resulting in an underestimation of particle-bound TEs with the ICP-TOF-MS setup. Thus, there is potential for increasing the sensitivity of the ICP-TOF-MS for particle-bound TEs by introducing a different inlet system.

[1] Pacyna, J and Pacyna, E, *Env. Reviews*, **9**, 269-298 (2001).

SECONDARY ORGANIC AEROSOL MARKERS IN THE FIESCHERHORN ICE CORE

A. Lauer, A. L. Vogel, F. Bachmeier (Goethe Univ.), K. Arturi, S. Bjelić (PSI LBK),
I. El Haddad (PSI LAC), L. Fang, M. Schwikowski (PSI & Univ. Bern)

Using a comprehensive non-target analysis, we were able to reconstruct the organic aerosol composition from glacier ice. Furthermore, we can estimate the contribution of biogenic and anthropogenic aerosol markers to the atmosphere from the pre-industrial to the industrial age.

Among others, secondary organic aerosols (SOA) affect the Earth's radiative balance and thus climate, alter biogeochemical cycles and can contribute to air quality and pollution [1]. Understanding the abundance, properties, and atmospheric transformation of organic aerosols, especially in the pre-industrial atmosphere, will help reduce uncertainties in climatic modeling [2]. Consequently, accurate predictions of trends in SOA concentration and distribution must be made. The dispersal and the chemical composition of atmospheric aerosols can be investigated through the analysis of water-soluble organic matter preserved in ice cores [3].

82 samples from an ice core of the Fiescherhorn glacier, located in the Bernese Alps in Switzerland, were analyzed. This ice core contains historical records of about 300 years (1682-2002) of deposited aerosols and organic gases [4]. The ice core samples were cut in the PSI cold-lab at -20°C , decontaminated, concentrated via solid phase extraction (SPE) and analyzed by UHPLC/(-)ESI-HRMS. The data were evaluated using a non-target method with the software MZmine 2.

As a result, a temporal representation of the composition of various organic aerosol tracers from the pre-industrial to the industrial age is obtained. In Fig. 1 time series of two biogenic monoterpene oxidation products (pinic acid and MBTCA (3-methyl-1,2,3-butane tricarboxylic acid)), two anthropogenic aerosol markers ($\text{C}_9\text{H}_{20}\text{O}_4\text{S}$ and $\text{C}_7\text{H}_7\text{NO}_3$) and one marker for "anthropogenic enhancement" from α -pinene oxidation under high inorganic pollution conditions ($\text{C}_{10}\text{H}_{17}\text{NO}_7\text{S}$) are shown. Our results show the significant increase of compounds containing sulfur and nitrogen since the beginning of the 20th century, especially since around 1940. From the 1970s on a reversed trend is seen. In contrast, biogenic tracers from monoterpene oxidation have high concentrations before 1900 when they start to decrease reaching a minimum around 1940. Afterwards concentrations increase again. Similar to the anthropogenic aerosol markers, pinic acid begins to decrease around 1970 whereas MBTCA continues to increase.

Thick annual layers in more recent ice core parts lead to short time periods covered by one sample, resulting in a large variability, whereas thin annual layers near bedrock result in long time periods covered by the samples in the pre-industrial ice core parts.

While the relative trends of single organic compounds can now be interpreted, care must be taken when comparing signal intensities of different compounds. Furthermore, one has to keep in mind that appropriate internal standards are only available for a few species, which introduces uncertainty of the final time series. Additionally, ice core parts consisting of firn may be contaminated with certain semi-volatile compounds due to the porous structure of the firn.

Interpreting the biogenic tracer records in view of environmental changes regarding temperature, land cover and CO_2 concentrations is ongoing.

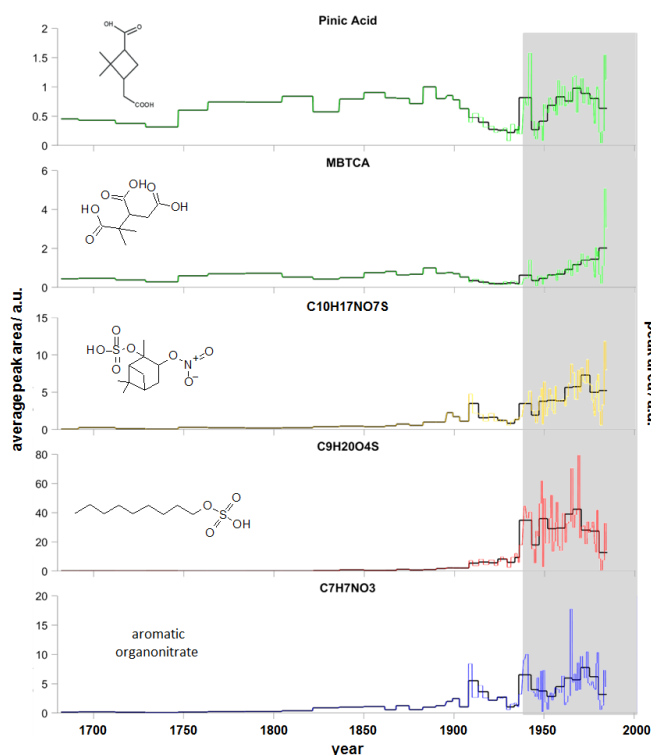


Fig. 1: Historic records of peak areas from different biogenic and anthropogenic aerosol markers. The grey area marks the firn samples.

We acknowledge the PSI Cross funding project "Reconstructions of pre-industrial organic aerosols" and the interlaboratory PostDoc project "Analysis of organic compounds from energy production to environment".

- [1] E. v. Schneidmesser et al., *Chem. Rev.*, **115**, 3856-3897 (2015).
- [2] K. S. Carslaw et al., *Nature*, **7474**, 67-71 (2013).
- [3] P. Fu et al., *Environ. Sci. Technol. Lett.*, **3**, 1514-1521 (2016).
- [4] T. M. Jenk et al., *Atmos. Chem. Phys.*, **612**, 5381-5390 (2006).

NOVEL ORGANIC COMPOUNDS IN THE BELUKHA ICE CORE

A. King (BAS & Univ. Cambridge), C. Giorio (Univ. Padova), M. Kalberer (Univ. Cambridge & Univ. Basel), M. Schwikowski (PSI & Univ. Bern), E. R. Thomas (BAS), E. Wolff (Univ. Cambridge)

The investigation of biogenic organic compounds in ice cores is a developing field which offers exciting potential for novel paleoclimate markers to be identified [1]. This study detects multiple novel organic compounds in samples dating back to 1598 from the Belukha Glacier ice core.

Analyses followed the method of King *et al.* [2], an optimized method of HPLC-MS analysis with sample pre-concentration by rotary evaporation. The list of target compounds is composed primarily of isoprene and monoterpene secondary oxidation aerosols (SOA), fatty acids, and primary biogenics.

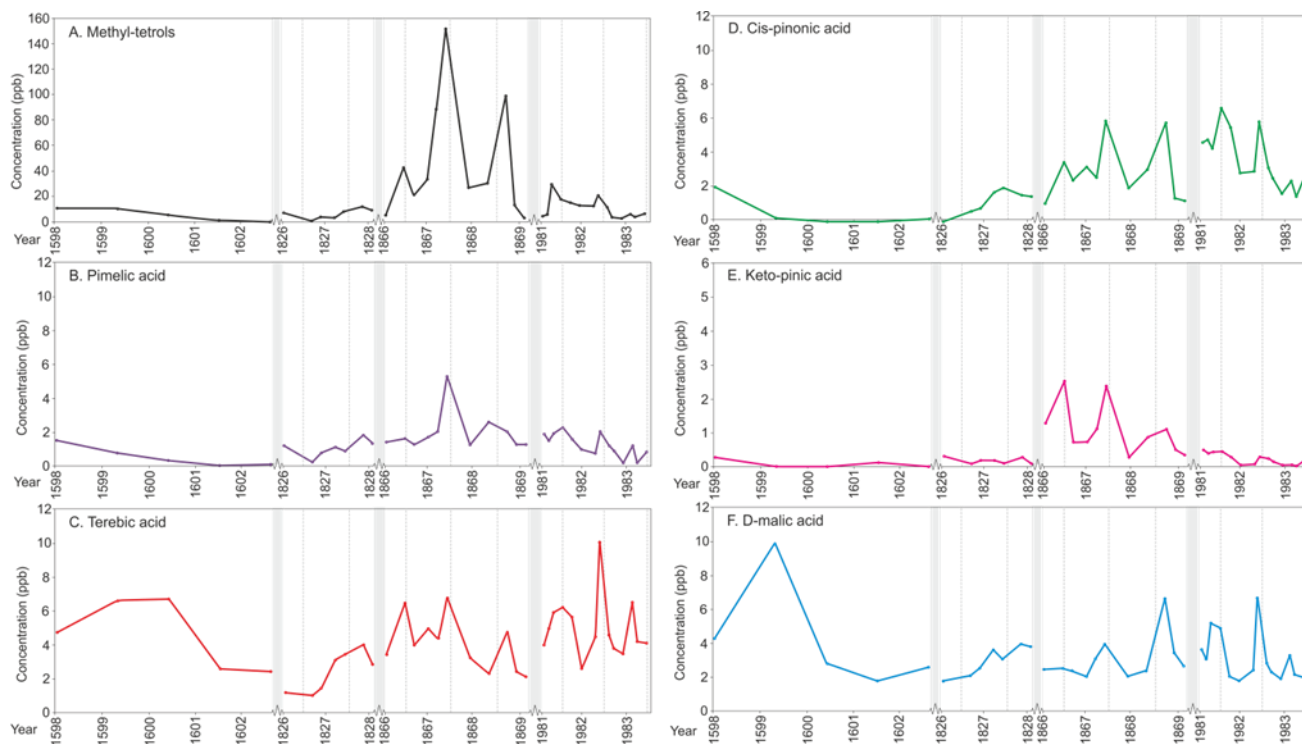
All compounds detected show strong seasonal cycles, where core resolution allows, with summer peaks in concentrations. Principle component analysis suggests a significant source-emission signal contributing to this seasonality for organic compounds. This is distinct from the strong transport component, which is the main driver for the summer increase in concentrations of both organics and major ions in the core. One group of organic compounds, pimelic acid, keto-pinonic acid, cis-pinonic acid (monoterpene SOA) and methyl-tetrols (isoprene SOA), all show increasing concentrations between 1598 and 1869 (Fig. 1), alongside gradually in-

creasing local temperatures controlled by solar radiation [3]. In the 1980's, the post-industrial period, where warming is instead primarily controlled by CO₂ emissions, concentrations of these compounds are significantly lower (except for cis-pinonic acid). These compounds correlate with ammonium in the periods before 1940, after which ammonium concentrations significantly increase due to dominant anthropogenic input [4]. Another group of organic compounds, terebic acid (monoterpene SOA) and D-malic acid (primary biogenic) instead shows high concentrations 1598-1602, a period when biomass burning was high [4]. The organic compounds in this study show the potential of multiproxy records for both source emissions of SOA compounds and biomass burning.

We acknowledge funding from a NERC DTP Grant NE/L002507/1.

- [1] C. Giorio *et al.*, *Quat. Sci. Rev.*, **183**, 1-22 (2018).
- [2] A. King *et al.*, *Talanta*, **194**, 233-242 (2019).
- [3] A. Eichler *et al.*, *Quat. Sci. Rev.*, **30**, 1027-1034 (2011).
- [4] A. Eichler *et al.*, *Geophys. Res. Lett.*, **36** (2009).

Fig. 1: Time series plots for organic compounds detected in the Belukha ice core. Note the different scales for (A) and (E) compared to (B), (C) and (D), as well as the decreasing sample resolution back in time. Dashed grey lines represent mid-year (summer) time points, and shaded grey boxes represent breaks in time.



300-YEAR ICE CORE RECORD OF DISSOLVED ORGANIC CARBON

L. Fang (PSI & Univ. Bern), A. L. Vogel (Goethe Univ.), T. M. Jenk (PSI), S. Szidat (Univ. Bern),
M. Schwikowski (PSI & Univ. Bern)

Alpine ice cores allow access to continuous records of atmospheric composition back to the pre-industrial era in the regions where the majority of humans live. Here, we present a continuous record of the dissolved organic carbon (DOC) concentration from Fiescherhorn ice core (Swiss Alps) over the period of 1680-1990. Fossil and non-fossil origins of water-soluble organic carbon in the past atmospheric aerosols were reconstructed based on radiocarbon source apportionment.

Even though organic aerosols may have a significant effect on cloud formation and climate, to our knowledge no data has been published on long-term changes in the organic aerosol fraction. Alpine glaciers are valuable archives for the past atmospheric compositions. However, investigation about organic aerosols from ice cores is challenging due to the vulnerability to contamination and the low concentration level [1]. Therefore, it is vital to ensure ultra-clean sample preparation and analysis procedures. The overall low blank and high efficiency of our DOC extraction setup makes it possible to analysis DOC in ice samples with a carbon content as low as $25 \mu\text{g C kg}^{-1}$ ice [2].

The 150.5 m long Fiescherhorn ice core (Swiss Alps) was drilled to bedrock in 2002 and well dated back to 1682 by annual layer counting. The average DOC concentration in the pre-industrial period (<1850) is around 96 ± 19 ppb, which is comparable with previously reported DOC concentrations in the Col du Dome ice core, French Alps, for the period 1920-1950 [1]. DOC decreased from 134 ppb in 1880s to 61 ppb in 1940s. After 1940, DOC raised again and reached up to about 300 ppb in the 1980s (Fig. 1).

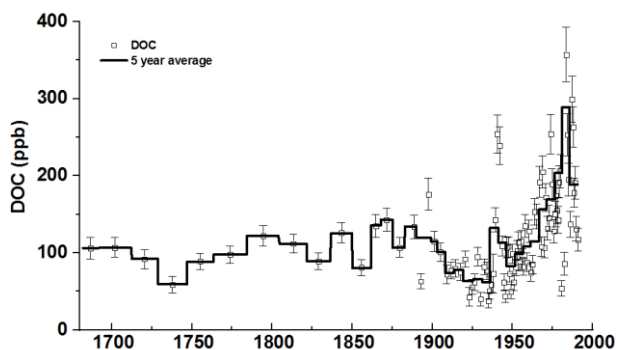


Fig. 1: Concentrations of DOC in the Fiescherhorn ice core. The individual samples are shown as circles with 1σ uncertainty. The line indicates 5-year averages after 1850, lower resolution before 1850.

Correcting DOC for formic acid and acetic acid, organic gases taken up during snowfall, we retrieved the water-soluble organic carbon (WSOC) [3], which represents the major fraction of the organic aerosol. The 10-year

average WSOC trend (after 1850) separated in the fossil and non-fossil contribution is shown in Fig. 2. This radiocarbon based source apportionment indicated that WSOC was of non-fossil (WSOC_{nf}) origin before 1850, with concentrations of about 75 ± 18 ppb. Anthropogenic fossil fuel input to WSOC (WSOC_{f}) increased since 1850 and reached non-fossil levels in the period 1960-1975. The fossil WSOC trend matches the estimated anthropogenic volatile organic compounds (AVOCs) emissions from Switzerland, suggesting that the fossil contribution is well preserved in the ice core. In contrast to the WSOC_{f} trend, WSOC_{nf} decreased from 97 ppb in the 1870s to 44 ppb in the 1940s, after which it raised again to pre-industrial levels at around 1970 and continued to increase until 1990. Our record suggests that fossil fuel emissions have significantly modified the organic aerosol since the 1850s, despite the fact that the non-fossil fraction dominated over the whole period. The overall increase of WSOC_{nf} after 1940 is most likely related to enhanced biogenic emissions driven by the temperature increase and/or changes in the atmospheric oxidation capacity, while the decrease after 1890 is so far unexplained.

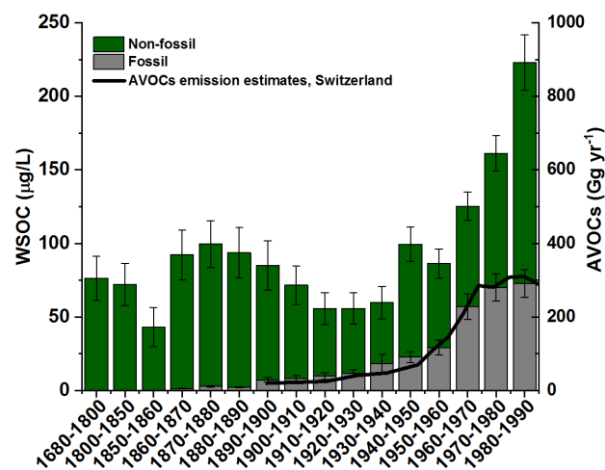


Fig. 2: WSOC concentrations from fossil and non-fossil sources over the period of 1680-1990. Error bar shows 1σ analysis uncertainty.

We acknowledge the Laboratory for the Analysis of Radiocarbon with AMS (LARA), especially Gary Salazar, for support with radiocarbon measurements.

- [1] M. Legrand et al. *Clim. Past*, **9**, 2195-2211 (2013).
- [2] L. Fang et al., *Radiocarbon*, in press.
- [3] M. Legrand et al., *J. Geophys. Res.*, **118**, 3879-3890 (2013).

DATING OF THE MT. HUNTER ICE CORE FROM ALASKA

L. Fang (PSI & Univ. Bern), D. Winski, K. Kreutz (Univ. Maine), T. M. Jenk (PSI),
M. Schwikowski (PSI & Univ. Bern)

A precise depth-age relationship of ice cores is essential for paleoclimate studies. In the Mt. Hunter ice core the annual layer signal could not be resolved anymore below a depth of 150 m w.eq. due to strong thinning. Based on radiocarbon dating of water insoluble organic carbon (WIOC), an age of 9198 ± 1160 BP was obtained at the depth of 169.2 m w.eq. A two-parameter flow model indicated the core to cover most of the Holocene.

The Mt. Hunter ice core was drilled in 2013 at 3900 m a.s.l in the saddle between the north and middle peaks of Mt. Hunter [1]. Determining mountain glaciers' age-depth relationship in the deeper part is challenging due to complex bedrock geometry and strong annual layer thinning. Here we report the chronology for the entire Mt. Hunter ice core by applying radiocarbon dating of WIOC and a two-parameter flow model (2-p model) [2].

12 samples were selected from the deeper part of the core. In order to remove any contamination potentially contained in the outer layer, we rinsed these ice samples with ultra-pure water in a flow hood. The carbonaceous particles were filtrated onto prebaked quartz fibre filters and combusted in a thermo-optical OC/EC analyzer (Model4L, Sunset Laboratory Inc, USA) at the University of Bern, following a well-established protocol (Swiss 4S) for OC/EC separation [2, 3]. ^{14}C analysis was conducted using the compact radiocarbon AMS system 'MICADAS' equipped with a gas ion source, directly coupled to the Sunset instrument.

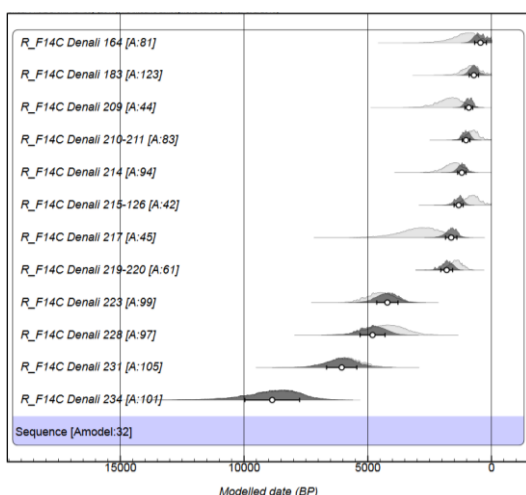


Fig. 1: Sequence of the calibrated ages for the Mt. Hunter ice core. Original and modelled age distributions are shown in light gray and dark gray, respectively. Open circles with error bars represent the mean age with 1σ uncertainty.

Conventional ^{14}C ages were calibrated using OxCal 4.3.2 and the IntCal13 calibration curve as shown in

Fig. 1 with calibrated ages given in years before present (BP). The so derived (original) age distributions have a relatively high uncertainty, especially for samples with a low ^{14}C content due to low carbon mass ($< 10 \mu\text{g C}$) or age. Better age constraint was achieved by applying the OxCal sequence model, valid under the assumption of increasing ages with depth. The range of calibrated ages in the Mt. Hunter ice core is from 380 ± 222 BP at 115.9 m w.eq. to 9198 ± 1160 BP at 169.2 m w.eq. (Fig. 1).

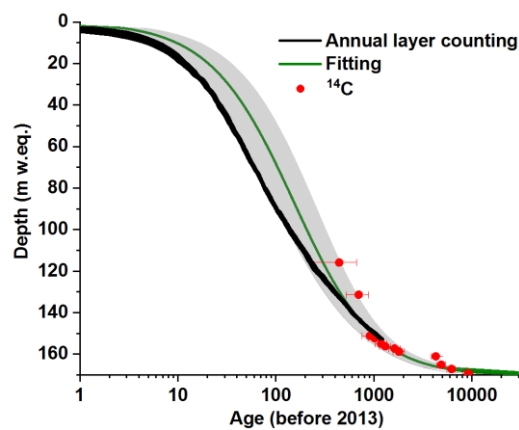


Fig. 2: The depth-age relationship of the Mt. Hunter ice core. 2-p model fit (green line) with 95% confidence band (grey). Calibrated ^{14}C ages with 1σ uncertainties are indicated by dots with error bars. The black band shows ages derived by annual layer counting with uncertainty estimates.

To retrieve a continuous depth-age relationship for the entire core, calibrated ^{14}C ages were fitted by a 2-p model [2] (Fig. 2). For the ice core section with overlapping dating from both, annual layer counting (ALC) and ^{14}C , the respectively obtained age-depth relationships are in excellent agreement considering the uncertainties. Note that the discrepancy between the 2-p model ages and the ages obtained by ALC in the upper 120 m w.eq. is explained by a change in annual accumulation rates observed over the respective time period. In this part, the model is not constrained by any data and it further assumes constant accumulation. Our ^{14}C dating suggests the bottom ice of the Mt. Hunter core to be from late Pleistocene origin, being preserved throughout the Holocene.

We acknowledge support from S. Szidat and the AMS laboratory at University of Bern (LARA).

- [1] D. Winski et al., Scientific Reports, **7**, 17869 (2017).
- [2] C. Uglietti et al., The Cryosphere, **10**, 3091-3105 (2016).
- [3] Y. L. Zhang et al., Atmos. Chem. Phys., **12**, 10841 (2012).

ACCUMULATION RATES FROM A REMOTE CENTRAL ASIAN GLACIER

M. Kronenberg (Univ. Fribourg), A. Eichler, S. Brüttsch (PSI), M. Hoelzle, H. Machguth (Univ. Fribourg), M. Schwikowski (PSI & Univ. Bern)

Firn core analysis of a melt-affected site in Central Asia provides recent annual accumulation rates and current firn characteristics. These results replenish the unique data set of a remotely located glacier in a data sparse region.

Only a few studies investigate the firn characteristics of mountain glaciers and firn core data is especially sparse for glaciers located in remote mountain ranges. Firn characteristics including stratigraphy and density profiles of such cores represent climate conditions and therefore indicate the evolution of the firn as a response to climate change [1]. Furthermore, accumulation rates derived from firn cores provide information about the mass balance of past years at the drilling site [2]. The identification of annual layers in a core may be hampered if melt water percolation occurs, as leaching processes change the chemical composition of the firn pack. The SNF project “Changing Glacier Firn in Central Asia and its Impact on Glacier Mass Balance” aims at identifying current firn characteristics of selected glaciers located in Kyrgyzstan compared to historical firn measurements, to subsequently identify possible firn changes and assess their potential effects on mass balance estimations.

Here, we present analyses results of a firn core, we drilled in February 2018 on Abramov Glacier at 4392 m a.s.l. (“core 4392”). Abramov glacier is located in the Pamir Alay in southern Kyrgyzstan and has a temperate accumulation area. The glacier was thoroughly investigated within the Soviet glaciological monitoring network from 1967 until 1999. In 2011, University of Fribourg and the Central Asian Institute for Applied Geosciences reinitiated glaciological measurements. Since 2013, the annual mass balance is measured at the drilling site and converted to meter water equivalent (m w.e.). Core4392 is 17 m long and was drilled with a KOVACS MarkII coring system. Core sections were shipped frozen to Switzerland and then cut into samples of ~8 cm length. Samples were analysed for major anions and cations, water stable isotopes and black carbon. Furthermore, the density of each sample and of the entire core segments and the visible stratigraphy were recorded (Fig.1), showing by the presence of ice lenses that repeated melt and refreezing takes place at the drilling site. Nevertheless, annual horizons were identified using mainly the seasonal signal of BC, ammonium and $\delta^{18}\text{O}$, supported by the visible stratigraphy (dust layers in orange Fig.1a). Obtained annual layer thickness in m w.e. agree well with the measurements at the same site for the period 2013-2015 (not shown). In 2016 and 2017, annual accumulation was measured in early August, before the end of the ablation season. Annual layer thickness obtained from the core indicate that there was

a mass loss of about 80 mm w.e. between the measurement date and the end of the ablation season for both years. This agrees well with a model-based temporal homogenization of the annual layer thickness measurements (not shown). Accumulation rates obtained from core4392 thus validate annual mass balance measurements since 2013 and allow extending the time series for two more years. We also measured several km of ground penetrating radar (GPR). The profiles clearly show layering in the firn, which is currently analysed and will be used to extrapolate the accumulation rates spatially. Furthermore, the GPR data also allows to link the results from core4392 to other nearby firn cores, which were analysed for visible stratigraphy and densities only. This will allow for a direct comparison to historical firn profiles.

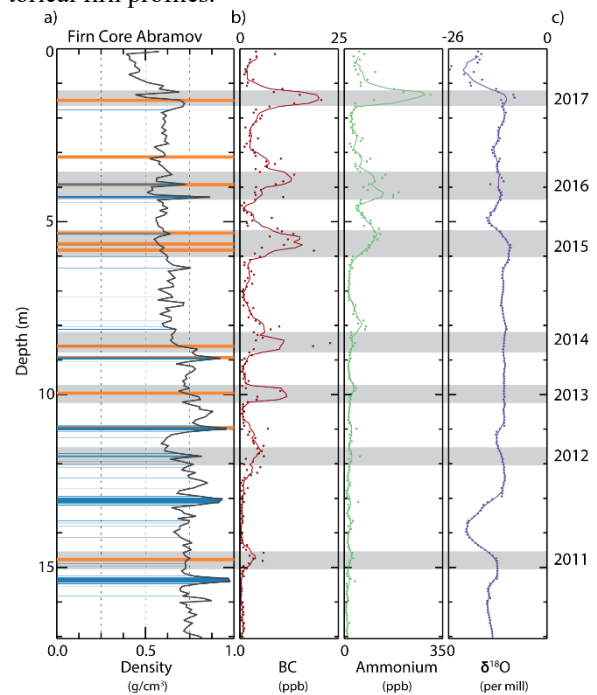


Fig. 1: Firn characteristics and chemical records of core4392. a) Firn stratigraphy (ice lenses in blue; visible dust layers in orange) and sample densities in black). b) Black carbon (BC), ammonium and $\delta^{18}\text{O}$ data are plotted as dots, lines show 5 point-moving averages. Identified summer horizons are shaded grey and labelled with their respective year (c).

We acknowledge funding from the Swiss National Science Foundation (Grant 200021_169453).

- [1] H. Machguth et al., *Nat. Clim. Chang.*, **6**, 390-395 (2016).
- [2] S. Sold et al., *The Cryosphere*, **9**, 1075-1087 (2015).

DRILLING OF TWO NEW ICE CORES FROM BELUKHA, SIBERIAN ALTAI

T. M. Jenk, M. Sigl, J. Stampfli (PSI), M. Barandun (Univ. Fribourg), R. Schild (PSI, hasliberge.ch), T. Papina, S. Eyrikh (IWEP), M. Schwikowski (PSI & Univ. Bern)

In a drilling expedition to the Siberian Altai (Russia, 20 May - 12 June 2018) two new ice cores were recovered from the glacier on Mount Belukha, extending the core previously drilled by our group in 2001, which has resulted in a broad range of published high quality climate and environmental records.

The study site in the Russian Altai represents one of the Earth's most continental regions. Approximately two thirds of Earth's boreal forest is located in Siberia. The ecosystems are mostly temperature controlled and the largest increases in temperatures are predicted for this area. A first drilling on Belukha glacier in 2001 (49°48'26.00"N, 86°34'43.00"E) did not reach bedrock, since the site had to be evacuated due to bad weather. The 139 m long ice core covering the time period AD 1250-2001 was investigated for a broad range of climatic and environmental conditions related to changes in both, natural and anthropogenic emissions, leaving no leftover ice for further studies of this highly interesting site [e.g. 1, 2]. A nearby ice core from the Belukha West Plateau obtained by Vladimir B. Aizen (University of Idaho) was dated by ¹⁴C of water-insoluble organic carbon at PSI indicating the presence of about 9'100 year old ice near bedrock [3].

The new ice cores were drilled on the saddle between the main summit (Belukha East) and the western peak of Mt. Belukha at an altitude of 4060 m a.s.l. (Fig. 1). The drilling itself took place between 27 May and 10 June, using the light-weight, portable, electromechanical ice core drilling device FELICS (8 cm core diameter) [4].

One core, denoted here as "2018 SNF", was drilled to up-date the 2001 PSI core to the present and to extent it from AD 1250 back in time. This was done in the framework of the project "Paleo fires from high-alpine ice cores", an integrated research frame work with the objective to advance the understanding of complex systemic linkages between climate, land use, fire and vegetation looking at the last 150 years in comparison to the previous 2000 years. The "2018 SNF" core was drilled around 90 m NE of the 2001 drill site, slightly south of the saddle plateau (49°48'27.7"N, 86°34'46.5"E). There, only slow glacier flow velocities and minimal ice strain was assumed while close to it maximal glacier thickness was expected (Fig. 2). This core of overall good quality reached bedrock at 160 m, with the used stainless steel drillhead hocking into the rock, thereby damaging the cable by twisting it.

The other core, denoted here as "2018 Ice Memory", was drilled first, only 14 m NE of the 2001 site (49°48'26.4"N, 86°34'43.4"E). This core was collected for the international program ICE MEMORY, aimed to

create the world's first ice archive sanctuary in Antarctica for preserving the memory of high-mountain glaciers threatened by global warming for future generations of scientists. The "2018 Ice Memory" core, the third core of the program, reached a depth of 106 m when drilling was abandoned after penetrating into a sub-glacial crevasse not visibly indicated on the surface.

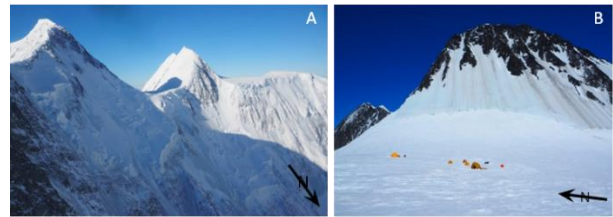


Fig. 1: (A) View of Mt. Belukha approaching by helicopter from NE. The drill site is located on the saddle between the main summit, Belukha East (to the left), and Belukha West. The Belukha West Plateau can be seen on the right side. (B) View of the saddle and Belukha main summit with camp and the drilling tent to the left (SNF site).

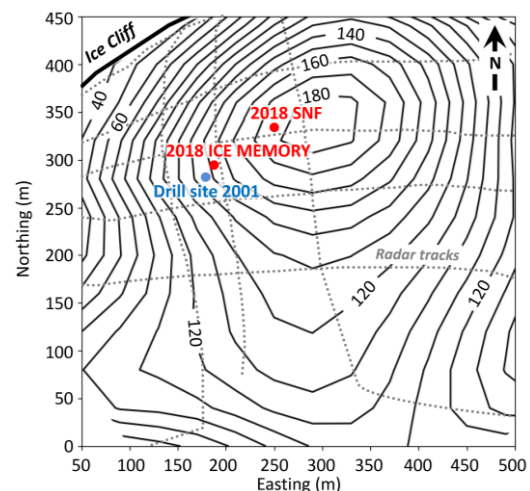


Fig. 2: Radar derived map of ice thickness (m) at the saddle with PSI ice core sites.

We acknowledge funding from the Swiss National Science Foundation (Sinergia, Grant 154450) and the Swiss Polar Institute. The ice thickness map was kindly provided by M. Lühti, University of Zürich.

- [1] A. Eichler et al., *Geophys. Res. Lett.*, **36**, L01808, (2009).
- [2] A. Eichler et al., *Quat. Sci. Rev.*, **30**, 1027-1034, (2011)
- [3] C. Uglietti et al., *The Cryosphere*, **10**, 3091-3105 (2016).

ARCTIC ICE NUCLEATING PARTICLES OVER THE LAST CENTURIES

M. Hartmann (TROPOS), T. Blunier (Univ. Copenhagen), S. O. Brügger (Univ. Bern), J. Schmale (PSI LAC), M. Schwikowski (PSI), A. L. Vogel (Goethe Univ.), H. Wex, F. Stratmann (TROPOS)

Atmospheric concentrations of Ice Nucleating Particles (INP) were derived from two Arctic ice cores. For the first time the historical record of those particles, which are key factors for the properties of Arctic mixed-phase clouds, has been assessed.

The Arctic is one of the regions most sensitive to climate change, and changes are proceeding at an unprecedented pace and intensity, which is referred to as Arctic Amplification [1]. Arctic peculiarities together with multiple feedback mechanisms, are known to contribute to the enhanced climate sensitivity of the Arctic. However, the relative importance, strength, and interconnection of these peculiarities and feedback mechanisms are still disputed [2]. Clouds with their specific microphysical properties, and the cloud phase (liquid water droplets or ice crystals) are one of the key factors in Arctic Amplification, because they affect the energy budget of the Arctic boundary layer. Ice Nucleation Particles (INP) are the prerequisite for the primary formation of ice in mixed-phase clouds, and affect the formation of precipitation, as well as life time, and radiative properties of clouds.

This study, for the first time to the knowledge of the authors, presents a historical record of ice nucleating particle concentrations (N_{INP}) for the past 500 years, derived from ice core material collected at two Arctic sites. The samples originate from the EUROCORE ice core (Summit, Central Greenland), and from the Lomo09 ice core (Lomonosovfonna, Svalbard). INP measurements were performed with the two droplet freezing arrays LINA (Leipzig Ice nucleation Array) and INDA (Ice Nucleation Droplet Array). The range of INP concentrations was found to be similar to present-day observations [3] and no overall trend was found. N_{INP} did not increase since the beginning of the industrialization, suggesting that anthropogenic pollution reaching the Arctic has no effect on N_{INP} . High onset temperatures for ice nucleation, and the general shape of the N_{INP} temperature spectra, indicate the presence of biogenic INP. For those, a local Arctic source, that is more active during particular times of the year, is likely. With the available data it is not possible to differentiate between marine or terrestrial sources. Although, the here presented historical record of Arctic INP concentrations does not exhibit a clear trend throughout the past 500 years, in view of Arctic Amplification, it has to be kept in mind, that the present changes in the Arctic are unprecedented in speed and intensity. New sources of highly ice active biogenic INP may arise or existing ones could be amplified [4].

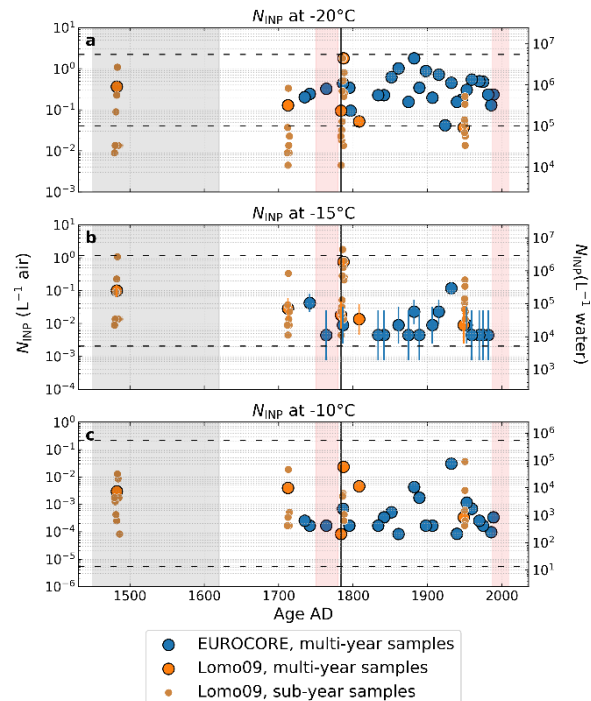


Fig. 1: Time series of N_{INP} at -20°C (panel a), -15°C (panel b), and -10°C (panel c) for multi- and sub-year samples at both sites. As a reference, black dashed horizontal lines are included which show the range of N_{INP} observed by [3] in precipitation samples for present North America and Europe. The shaded grayish area delineates a period of reduced Arctic ice extent found by [5] and shaded reddish areas show intervals of particularly warm summers on Svalbard by [6]. The black vertical line indicates the period of the 1783 Laki eruption as defined in [7].

We acknowledge the funding by the Deutsche Forschungsgemeinschaft (DFG, German Research Foundation) – Projektnummer 268020496 – TRR 172, within the Transregional Collaborative Research Center “Arctic Amplification: Climate Relevant Atmospheric and Surface Processes, and Feedback Mechanisms (AC)”.

- [1] M. C. Serreze et al., *Glob. Planet. Change*, **77**, 85-96 (2011).
- [2] A. J. Pithan et al., *Nat. Geosci.*, **7**, 181-4 (2014).
- [3] M. Petters et al., *Geophys. Res. Lett.*, **42**, 8758-8766 (2015).
- [4] K. R. Arrigo et al., *Geophys. Res. Lett.*, **35** (2008).
- [5] C. Kinnard et al., *Nature*, **479**, 509-512 (2011).
- [6] W. J. D’Andrea et al., *Geology*, **40**, 1007-1010 (2012).
- [7] R. J. Fiacco et al., *Quat. Res.*, **42** (1994).

GIRLS ON ICE SWITZERLAND – FIELD BASED SCIENCE COURSES FOR YOUNG WOMEN

M. Kronenberg (Univ. Fribourg, PSI), L. Hellmann, M. Habermann (PSI), K. Naegeli, M. Schwikowski (PSI & Univ. Bern)

Girls on Ice Switzerland provides unique, tuition-free wilderness science expeditions for young women from diverse backgrounds. In July 2018, nine teenage girls explored Findelen glacier during eight days, and analysed and presented their data to the public at PSI thereafter.

During a “Girls on Ice Switzerland” expedition, young women (15-17 years) become acquainted with science and scientific methods and learn about alpine climate change. Furthermore, they are introduced to art concepts and mountaineering, which is necessary for scientific fieldwork in an alpine environment. The female instructor team consists of two to three scientists and a mountain guide. During one day, visiting scientists (Fig. 1) and an artist share their expertise with the expedition team. “Girls on Ice Switzerland” is organised as an association and runs the courses in collaboration with the PSI. Between 2017 and 2020, Girls on Ice Switzerland is funded through a science communication (Agora) project of the Swiss National Science Foundation. During the courses, a mixture of inquiry-based teaching and experimental learning is applied. This combination and the tangibility of climate change science in the alpine environment provide a unique teaching ambience. Furthermore, the purely female environment creates an atmosphere in which the teenage girls lose their shyness to try out, learn and understand new things from domains, which are often perceived as male-dominated. The participants improve their mountaineering and outdoor skills and are taught the theoretical background necessary for different “peak” experiences: A central part of the programme are the students’ experiments. In groups of three, supervised by an instructor, the participants plan and carry out their own scientific experiment. After the field camp, they analyse their data at PSI and present their results to the public. Basic mountaineering skills are not only necessary to acquire the data, but also to climb a peak towards the end of the expedition. In addition to these challenging experiences, each participant has to take over a series of tasks to facilitate the daily routine in the base camp far away from civilisation. The camp is the place, where lively discussions come alive each night. Even the quietest ones are encouraged to participate, share their opinion and discuss the (philosophical) question asked each morning. The young women improve their reflection skills and discussion culture. Last summer, nine teenage girls with very distinct backgrounds built up the expedition team: Some of them were experienced camp organisers or rock climbers; others had taken numerous science classes before. There were extroverted entertainers and silent listeners. Each of them contributed her strengths and the team grew together to manage challenging situations as a group: The weaker ones were encouraged to

reach the peak. And almost nothing was left for the volunteering women who came up the mountain to carry down material, because the girls distributed everything perfectly well amongst each other.

“Girls on Ice” does not only exist in Switzerland. The scientific expeditions for teenage girls originate in the USA, where such courses were firstly organised almost 20 years ago. Under the umbrella of the NGO “Inspiring Girls Expeditions” numerous field trips with different scientific foci such as glaciology or geology are organised each year. The Swiss association is financially independent, but in close contact and coordinates its activities with the American organisation. In 2019, “Girls on Ice Switzerland” will organise two expeditions. The first edition for French-speaking participants will take place in addition to the German-language expedition. Find more information about the planned expeditions online [1]. The public presentations 2019 as well as possibilities how to support “Girls on Ice Switzerland” will be announced on the webpage and our social media channels.



Fig. 1: Margit Schwikowski joined the expedition team as a visiting scientist and explained how to use a portable ice drill.

We acknowledge funding from the Swiss National Science Foundation (Agora CRAGP2_171620).

[1] <http://www.inspiringgirls.org/switzerland>

LIST OF PUBLICATIONS

SURFACE CHEMISTRY

- P. Corral Arroyo, K. T. Malecha, M. Ammann and S. A. Nizkorodov
Influence of humidity and iron(III) on Photodegradation of atmospheric secondary organic aerosol particles
Physical Chemistry Chemical Physics **20**, 30021-30031, doi: 10.1039/C8CP03981J
- P. Corral Arroyo, T. Bartels-Rausch, P. A. Alpert, S. Dumas, S. Perrier, C. George and M. Ammann
Particle-phase photosensitized radical production and aerosol aging
Environmental Science and Technology **52** (14), 7680-7688, doi: 10.1021/acs.est.8b00329
- A. R. Cox, M. Ammann, J. N. Crowley, H. Herrmann, M. E. Jenkin, V. F. McNeill, A. W. Mellouki, M. J. Rossi, J. Troe, and T. J. Wallington
IUPAC In the (real) clouds – 40 years of evaluating atmospheric chemistry data
Chemistry International **40** (4), 10-13, doi: 10.1515/ci-2018-0404, 2018
- D. A. Knopf, P. A. Alpert and B. Wang
The role of organic aerosol in atmospheric ice nucleation: a review
ACS Earth and Space Chemistry **2** (3), 168-202, doi: 10.1021/acsearthspacechem.7b00120
- X. Kong, M. J. Wolf, M. Roesch, E. S. Thomson, T. Bartels-Rausch, P. A. Alpert, M. Ammann, N. L. Prisle and D. J. Cziczo
A continuous flow diffusion chamber study of sea salt particles acting as cloud nuclei: deliquescence and ice nucleation
Tellus B: Chemical and Physical Meteorology **70**, 1-11, doi: 10.1080/16000889.2018.1463806
- G. Li, H. Su, U. Kuhn, H. Meusel, M. Ammann, M. Shao, U. Pöschl and Y. Cheng
Technical note: Influence of surface roughness and local turbulence on coated-wall flow tube experiments for gas uptake and kinetic studies
Atmospheric Chemistry and Physics **18**, 2669-2686, doi: 10.5194/acp-18-2669-2018
- A. Waldner, L. Artiglia, X. Kong, F. Orlando, T. Huthwelker, M. Ammann and T. Bartels-Rausch
Pre-melting and the adsorption of formic acid at the air-ice interface at 253 K as seen by NEXAFS and XPS
Physical Chemistry Chemical Physics **20**, 24408-24417, doi: 10.1039/C8CP03621G

ANALYTICAL CHEMISTRY

- S. E. Avak, M. Schwikowski and A. Eichler
Impact and implications of meltwater percolation on trace element records observed in a high-Alpine ice core
Journal of Glaciology **64**, 877-886, doi: 10.1017/jog.2018.74
- S. O. Brügger, E. Gobet, M. Sigl, D. Osmont, T. Papina, N. Rudaya, M. Schwikowski and W. Tinner
Ice records provide new insights into climatic vulnerability of Central Asian forest and steppe communities
Global and Planetary Change **169**, 188-201, doi: 10.1016/j.gloplacha.2018.07.010
- S. O. Brügger, E. Gobet, F. Schanz, O. Heiri, C. Schwörer, M. Sigl, M. Schwikowski and W. Tinner
A quantitative comparison of microfossil extraction methods from ice cores
Journal of Glaciology **64**, 432-442, doi: 10.1017/jog.2018.31
- A. Dal Farra, S. Kaspari, J. Beach, T. D. Bucheli, M. Schaepman and M. Schwikowski
Spectral signatures of submicron scale light-absorbing impurities in snow and ice using hyperspectral microscopy
Journal of Glaciology **64**, 377-386, doi: 10.1017/jog.2018.29
- A. Gilgen, C. Adolf, S. O. Brügger, L. Ickes, M. Schwikowski, J. F. N. Van Leeuwen, W. Tinner and U. Lohmann
Implementing microscopic charcoal particles into a global aerosol-climate model
Atmospheric Chemistry and Physics **18**, 11813-11829, doi: 10.5194/acp-18-11813-2018

- M. M. Grieman, M. Aydin, E. Isaksson, M. Schwikowski and E. S. Saltzman
Aromatic acids in an Arctic ice core from Svalbard: a proxy record of biomass burning
Climate of the Past **14**, 637-651, doi: 10.5194/cp-14-637-2018
- P. D. Henne, M. Bigalke, U. Büntgen, D. Colombaroli, M. Conedera, U. Feller, D. Frank, J. Fuhrer, M. Grosjean, O. Heiri, J. Luterbacher, A. Mestrot, A. Rigling, O. Rössler, C. Rohr, T. Rutishauser, M. Schwikowski, A. Stampfli, S. Szidat, J.-P. Theurillat, R. Weingartner, W. Wilcke and W. Tinner
An empirical perspective for understanding climate change impacts in Switzerland
Regional Environmental Change **18**, 205-221, doi: 10.1007/s10113-017-1182-9
- S. Hou, T. M. Jenk, W. Zhang, C. Wang, S. Wu, Y. Wang, H. Pang and M. Schwikowski
Age ranges of the Tibetan ice cores with emphasis on the Chongce ice cores, western Kunlun Mountains
The Cryosphere **12**, 2341-2348, doi: 10.5194/tc-12-2341-2018
- D. Osmont, I. A. Wendl, L. Schmidely, M. Sigl, C. P. Vega, E. Isaksson and M. Schwikowski
An 800-year high-resolution black carbon ice core record from Lomonosovfonna, Svalbard
Atmospheric Chemistry and Physics **18**, 12777-12795, doi: 10.5194/acp-18-12777-2018
- M. Sigl, N. J. Abram, J. Gabrieli, T. M. Jenk, D. Osmont and M. Schwikowski
19th century glacier retreat in the Alps preceded the emergence of industrial black carbon deposition on high-alpine glaciers
The Cryosphere **12**, 3311-3331, doi: 10.5194/tc-12-3311-2018
- C. P. Vega, E. Isaksson, E. Schlosser, D. V. Divine, T. Martma, R. Mulvaney, A. Eichler and M. Schwikowski
Variability of sea salts in ice and firn cores from Fimbul Ice Shelf, Dronning Maud Land, Antarctica
The Cryosphere **12**, 1681-1697, doi: 10.5194/tc-12-1681-2018

AFFILIATION INDEX

BAS	British Antarctic Survey, High Cross, Madingley Road, Cambridge CB3 0ET, UK
CECS	Centro de Estudios Científicos, Arturo Prat 514, Valdivia, Chile
EMPA	Materials Science and Technology, Überlandstrasse 129, 8600 Dübendorf, Switzerland
ETHZ	Eidgenössische Technische Hochschule Zürich, 8092 Zürich, Switzerland
Goethe Univ.	Goethe-Universität, Campus Riedberg, Altenhöferallee 1, 60438 Frankfurt/Main, Germany
hasliberge.ch	Reto Schild, Schrändli 459, 6086 Hasliberg Reuti, Switzerland
IWEP	Institute for Water and Environmental Problems, Chemical Analytical Centre 1, Molodezhnaya str. Barnaul 656038, Russia
KUP, Univ. Bern	Klima und Umwelphysik (Climate and Environmental Physics), Universität Bern, Sidlerstrasse 5, 3012 Bern, Switzerland
LAC	Laboratory of Atmospheric Chemistry, Paul Scherrer Institut, 5232 Villigen, Switzerland
LBK	Bioenergy and Catalysis Laboratory, Paul Scherrer Institut, 5232 Villigen, Switzerland
LMN	Laboratory for Micro and Nanotechnology, Paul Scherrer Institut, 5232 Villigen, Switzerland
LSC	Laboratory for Condensed Matter, Paul Scherrer Institut, 5232 Villigen, Switzerland
LSK	Laboratory for Catalysis and Sustainable Chemistry, Paul Scherrer Institut, 5232 Villigen, Switzerland
LUC	Laboratory of Environmental Chemistry, Paul Scherrer Institut, 5232 Villigen, Switzerland
PKU	Peking University, No. 5 Yiheyuan Road, Haidian District, Beijing 100871, China
PSI	Paul Scherrer Institut, Forschungsstrasse 111, 5232 Villigen, Switzerland
TROPOS	Leibniz-Institut für Troposphärenforschung, Permoserstrasse 15, 04318 Leipzig, Germany
Univ. Basel	Universität Basel, Departement Umweltwissenschaften, Klingelbergstrasse 27, 4056 Basel, Switzerland
Univ. Bern	Universität Bern, Departement für Chemie und Biochemie, Freiestrasse 3, 3012 Bern, Switzerland
Univ. Cambridge	University of Cambridge, Selwyn College, Grange Road, Cambridge, CB3 9DQ, UK
Univ. Copenhagen	University of Copenhagen, Nørregade 10, 1017 Copenhagen, Denmark
Univ. Fribourg	Université de Fribourg, Avenue de l'Europe 20, 1700 Fribourg, Switzerland
Univ. Helsinki	University of Helsinki, Fabianinkatu 33, 00014 University of Helsinki, Finland
Univ. Maine	The University of Maine, School of Earth and Climate Sciences, 5790 Bryand Global Sciences Center, Orono, ME 04469-5790, USA
Univ. Oulu	University of Oulu, Pentti Kaiteran katu 1, 90014 University of Oulu, Finland
Univ. Padova	Università degli Studi di Padova, Via 8 Febbraio, 2, 35122 Padova, Italy
Univ. Tampere	Tampere University, Kalevantie 4, 33100 Tampere, Finland
WSL-SLF	Swiss Federal Institute for Forest, Snow and Landscape Research WSL, 8903 Birmensdorf, Switzerland
XMU	Xiamen University, No. 422, Siming South Road, Xiamen, Fujian, China 361005

